Influence of sand density and retaining wall stiffness on the three-dimensional responses of a tunnel to basement excavation

C.W.W. Ng[1], Jiangwei Shi[2], David Mašín[3], Huasheng Sun[4], and G.H. Lei[5]

An article submitted to CGJ for consideration of possible publication

Corresponding author: Mr Jiangwei Shi
Research student, Department of Civil and Environmental Engineering, Hong Kong University of Science and Technology, Clear Water Bay, Kowloon, Hong Kong.
E-mail: shijiangwei@ust.hk
Tel: 852-6762-9710

Co-author: Dr C. W. W. Ng
Chair Professor, Department of Civil and Environmental Engineering, Hong Kong University of Science and Technology, Clear Water Bay, Kowloon, Hong Kong.
E-mail: cecwwng@ust.hk
Tel: 852-2358-8760
Fax: 852-2358-1534

Co-author: Dr David Mašín
Associate Professor, Department of Engineering Geology, Institute of Hydrogeology, Engineering Geology and Applied Geophysics, Faculty of Science, Charles University in Prague, Prague, Czech Republic.
E-mail: masin@natur.cuni.cz

Co-author: Mr Huasheng Sun
Research Student, Key Laboratory of Geomechanics and Embankment Engineering of the Ministry of Education, Geotechnical Research Institute, Hohai University, 1 Xikang Road, Nanjing, China.
E-mail: sunhuadasheng@126.com

Co-author: Dr G.H. Lei
Professor, Key Laboratory of Geomechanics and Embankment Engineering of the Ministry of Education, Geotechnical Research Institute, Hohai University, 1 Xikang Road, Nanjing, China.
E-mail: leiguohui@hhu.edu.cn

ABSTRACT: Basement excavation inevitably causes stress changes in the ground leading to soil movements which may affect the serviceability and safety of adjacent tunnels. Despite paying much attention to the basement-tunnel interaction, previous research has mainly focused on the influence of tunnel location in relation to the basement, tunnel stiffness and excavation geometry. The effects of sand density and basement wall stiffness on nearby tunnels due to excavation, however, have so far been neglected. A series of three-dimensional centrifuge tests were thus carried out in this study to investigate these effects on the complex basement-tunnel interaction. Moreover, three-dimensional numerical analyses and a parametric study by adopting hypoplastic sand model were conducted to improve the fundamental understanding of this complex problem and calculation charts were developed as a design tool. When the basement was constructed directly above the existing tunnel, excavation-induced heave and strain were more sensitive to a change in soil density in the transverse direction than that in the longitudinal direction of the tunnel. Because a looser sand possesses smaller soil stiffness around the tunnel, the maximum tunnel elongation and transverse tensile strain increased by more than 20% as the relative sand density decreased by 25%. Moreover, the tensile strain induced along the longitudinal direction was insensitive to the stiffness of the retaining wall, but that induced along the transverse direction was significantly reduced by a stiff wall. When the basement was constructed at the side of the existing tunnel, the use of a diaphragm wall reduced the maximum settlements and tensile strains induced in the tunnel by up to 22% and 58%, respectively, compared with the use of a sheet pile wall. Under the same soil density and wall stiffness, excavation induced maximum movement and tensile strains in the tunnel located at a side of basement were about 30% of the measured values in the tunnel located directly beneath basement centre.

KEYWORDS: three-dimensional responses, basement excavation, tunnel, sand density, retaining wall stiffness, calculation chart

INTRODUCTION

With an increasing demand for new infrastructures in congested urban cities, underground constructions such as deep excavations have become commonplace. For public convenience, basement excavations for shopping malls and/or car parks are done very close to existing tunnels (within a distance of 0.5 times the tunnel diameter as reported by Burford (1988) and Liu et al. (2011)). But any basement excavations cause stress changes in the ground leading to soil movements which may in turn induce unacceptable deformations and stress changes in adjacent tunnels.

To evaluate the basement-tunnel interaction, several researchers simplified it as a plane strain problem (Doležalová, 2001; Sharma et al., 2001; Hu et al., 2003; Karki, 2006; Zheng and Wei, 2008). Sharma et al. (2001) conducted a two-dimensional numerical analysis to investigate tunnel deformation due to adjacent basement excavation. They found that tunnel deformation decreased with an increase in lining stiffness. Zheng and Wei (2008) carried out a plane strain numerical parametric study to investigate tunnel deformation and stress redistribution around the tunnel lining due to basement excavation. They found that the tunnel deformation mode was closely related to the distance between the tunnel and the retaining wall. Other researchers have shown that movement and bending moment are induced in a tunnel not only along its transverse direction but also along its longitudinal direction as a result of basement excavation (Lo and Ramsay, 1991; Chang et al., 2001; Meguid et al., 2002; Huang et al., 2012, 2013; Ng et al., 2013b; Shi et al., 2015). Due to corner effects in a short and narrow excavation, it is expected that excavation induced tunnel responses at basement centre would be different from those under the plane strain condition. By conducting a numerical parametric study, Shi et al (2015) investigated three-dimensional tunnel heave and tensile strain to overlying basement excavation. Influence of excavation geometry, sand density, tunnel stiffness and joint stiffness on the basement-tunnel interaction was explored.

Huang et al. (2012) carried out a series of three-dimensional centrifuge tests in Shanghai soft clay to investigate the effect of the cover-to-diameter ratio (C/D) on a tunnel's responses to overlying basement excavation. The measured maximum tunnel heave was found to decrease exponentially with an increase in the C/D ratio. However, they did not measure the bending moments in the tunnel along its longitudinal direction. Huang et al. (2013) conducted a three-dimensional numerical parametric study to investigate the basement-tunnel interaction using the Hardening Soil model to simulate soil responses. It is well-known that soil stiffness is not only strain dependent but also stress path dependent (e.g., Atkinson et al., 1990; Powrie et al., 1998), but the HS model is unable to capture their effects on soil stiffness.

Ng et al. (2013b) conducted two three-dimensional centrifuge tests in sand to investigate the influence of basement excavation on an existing tunnel located in either of two horizontal offsets in relation to the basement. Basement excavations were carried out in medium-dense sand with relative densities of 68% and 69%. A maximum heave of 0.07% H_e (final excavation depth) and settlement of 0.014% H_e were induced in the tunnel when the basement was excavated directly above the tunnel and when it was constructed at the side of the tunnel, respectively. Vertical elongation was induced in the tunnel in the former case, while distortion was observed in the tunnel in the latter case. An inspection of the measured strains in the tunnel along its longitudinal direction revealed that the inflection point, i.e. the point where the shear force was at a maximum, was located 0.8 L (basement length) away from the basement centre.

Despite paying much attention to the basement-tunnel interaction, previous studies have mainly focused on the influence of tunnel location in relation to the basement, and the effects of excavation geometry and tunnel stiffness. The effects of strain and stress path dependencies on soil stiffness, however, were often not considered. As the sand density is reduced, vertical stress relief at the formation level of the basement and soil stiffness around the tunnel decrease simultaneously. But tunnel responses dominated by reduced stress relief or soil stiffness were not clear. By collecting 300 case histories, Wang et al. (2010) found that the mean values of the maximum lateral movement of a sheet pile wall and a diaphragm wall as a result of basement excavation were 1.5% H and 0.27 % H, respectively, where H was excavation depth. Thus, the responses of a tunnel located behind a retaining wall may be significantly affected by wall flexural stiffness.

This paper is a continuation of a previous paper (Ng et al., 2013b) and considers the influence of sand density and retaining wall stiffness on three-dimensional responses of a tunnel to basement excavation. Four three-dimensional centrifuge tests were thus designed and conducted to investigate these effects on the basement-tunnel interaction. In addition, three-dimensional numerical back-analyses were carried out to enhance the fundamental understanding of stress transfer mechanisms and soil stiffness around the tunnel. Moreover, a three-dimensional numerical parametric study was conducted to determine the effects of wall stiffness on the complex interaction. To capture the effects of strain and stress path dependencies on soil stiffness, an advanced constitutive model, namely the hypoplastic sand model, was adopted in the numerical analyses.

THREE-DIMENSIONAL CENTRIFUGE MODELLING

Experimental program and set-up

Four three-dimensional centrifuge tests were designed and conducted at the Geotechnical Centrifuge Facility of the Hong Kong University of Science and Technology. The 400 g-ton centrifuge has an arm radius of 4.2 m (Ng et al., 2001, 2002). In order to have enough space for installing instruments (i.e., potentiometer and strain gauge) inside the tunnel lining, the diameter of the model tunnel cannot be too small. By considering boundary conditions of entire model package, the model tunnel with a diameter of 100 mm was adopted in this study. In order to simulate tunnels commonly constructed in many urban cities such as Taipei, London and Shanghai (e.g., Chang et al., 2001; Mohamad et al., 2010; Sun et al., 2012; Wang et al., 2014), 60 g (i.e., gravitational acceleration) was chosen to give a corresponding 6 m diameter (in prototype) tunnels. The dimensions of soil were 1245 mm (length) × 990 mm (width) × 750 mm (depth). According to the relevant scaling laws summarised in Table 1 (Taylor, 1995), the dimensions of the soil stratum were equivalent to 74.7 m (length), 59.4 m (width) and 45.0 m (depth) in prototype.

Due to time and budget constraints, it is not realistic to conduct centrifuge tests for every case. For a tunnel located directly underneath basement centre, centrifuge tests were designed and carried out to investigate the influence of sand density on the basement-tunnel interaction. On the other hand, numerical parametric study was conducted to explore the influence of wall stiffness on tunnel responses by overlying excavation, instead of carrying out centrifuge model tests.

For a tunnel located at a side of basement, excavation induced tunnel responses were negligible when a diaphragm wall was used as the retaining system (Ng et al., 2013b). In order to explore tunnel responses when a less stiff retaining system was adopted, one test was designed to use a sheet pile wall. Similarly, numerical parametric study was decided and carried out to investigate the effects of sand density to save time and budget. Detailed measurements in the tests are presented in following sections.

Figure 1 shows a plan view of the centrifuge model. The model wall and tunnel were assumed to be wished-in-place in each test. A square excavation (on plan) with a side length of 300 mm (18 m in prototype) was carried out. In the four tests, the distance between the model wall and the boundary of the container was no less than 2.2 times the final excavation depth (2.2 H_e), which was larger than the influence zone (i.e., 2 H_e) of ground settlement behind the retaining wall identified by Peck (1969) for basement excavation in sand. Tests CD51 and CD68 (with relative sand densities of 51% and 68%, respectively) were designed to investigate the effects of soil density on the basement-tunnel interaction when the basement was excavated directly above the tunnel. The diaphragm wall (DW) and the sheet pile wall (SW) are both typical retaining systems for basement excavation. The sheet pile wall is used to support basements worldwide provided the final excavation depth is less than 12 m (e.g., Hsieh and Ou, 1998; Long, 2001; Wang et al., 2010). In Tests CD51, CD68 and SD69, the diaphragm wall was used as the retaining system, while the sheet pile wall was installed to support the basement in Test SS70. By comparing soil and tunnel responses in Tests SD69 and SS70, the effects of retaining wall stiffness on the basement-tunnel interaction were explored. In these two tests, the model tunnel was located at the side of the basement with a clear distance between its springline and the basement of 25 mm (1.5 m in prototype). Note that the measured results of Tests CD68 and SD69 have been reported by Ng et al. (2013b). A summary of the four centrifuge tests is given in Table 2.

Figures 2a & b show elevation views of the centrifuge model. The final excavation depth (H_e) was 150 mm, corresponding to 9 m in prototype. The wall penetration depth in model scale was 75 mm which was half the final excavation depth and exceeded the clear distance between the tunnel crown and the formation level of the basement (50 mm). Thus, two arches were made in the walls to accommodate the tunnel in Tests CD51 and CD68 (see Fig. 2b). The clear distance between the tunnel crown and the arches was 20 mm which was equivalent to 1.2 m in prototype. Such set-ups have been reported by several researchers (e.g., Liu et al., 2011; Huang et al., 2012, 2013; Ng et al., 2013b). In this study, basement excavation was simulated by draining away heavy fluid ($ZnCl_2$). Because of its simplicity, heavy fluid is commonly used to simulate the effects of excavation by draining the fluid away in-flight (e.g., Bolton and Powrie, 1988; Leung et al., 2001, 2003; Zheng et al., 2012). By doing so, in-situ horizontal stress may not be simulated correctly if the coefficient of earth pressure at rest (K_0) is not equal to 1. For the tests reported in this paper, K_0 of sand was estimated as 0.5 by using the equation proposed by Jáky (1944). Thus, the horizontal stress acting on retaining wall was over released in this study. However, this over relaxation should not affect major conclusions drawn from this study. This is because the effects of excavation on an existing tunnel located below it should be governed mainly by the vertical stress rather than the horizontal stress relief. The excavation proceeded in three stages where a depth of 50 mm (3 m in prototype) was excavated in each stage. The diameter and initial cover depth of the model tunnel were 100 and 200 mm (6 and 12 m respectively in prototype), giving a tunnel cover-to-diameter ratio (C/D) of 2. The distance from the tunnel invert to the bottom of the model box was 0.45 m (4.5 D) which was equivalent to 27 m in prototype.

Model wall and tunnel

In all tests, the model wall and tunnel were made from single sheets and a tube of aluminium alloy, respectively. The influence of joints in the wall and the tunnel was beyond the scope of this study. In Tests CD51, CD68 and SD69, the aluminium sheets were 12.7 mm thick and were equivalent to 0.96 m thick concrete walls in prototype, assuming Young's modulus (E_{concrete}) of concrete of 35 GPa. On the other hand, 4 mm thick aluminium sheets were used to simulate a typical U-type sheet pile wall (i.e., type NSP III with moment of inertia of 3.24×10^{-4} m^4/m in prototype) in Test SS70. The flexural stiffness (E_wI_w) of the diaphragm wall was 32 times that of the sheet pile wall.

The model tunnel was 1200 mm long, 100 mm wide and 3 mm thick, corresponding to 72, 6 and 0.18 m in prototype, respectively. At 60 g, it had longitudinal stiffness and transverse stiffness equivalent to those of 420 and 230 mm thick concrete slabs ($E_{concrete}$ = 35 GPa), respectively.

Model preparation

Considering the complexity of the basement-tunnel interaction, dry Toyoura sand was adopted in the tests for simplicity. Dry Toyoura sand is a uniform fine sand with a mean grain size (D_{50}) of 0.17 mm and a specific gravity (G_s) of 2.65 (Ishihara, 1993).

Figure 3a shows the centrifuge model with strain gauge and potentiometer instruments installed. The pluvial deposition method was used to prepare soil samples. By keeping the hopper at constant distances of 200 and 500 mm above the sand surface, repeatable relative sand densities of about 50% and 70% were achieved in the calibration, respectively. The model tunnel with extension rods was installed once the sand had reached the invert level. An enlarged base was fixed at the bottom of each extension rod via a screw to increase the contact area between the rod and the outer surface of the tunnel lining. Each extension rod was protected by a hollow tube from the surrounding sand to minimise friction and was connected to a linear variable differential transformer (LVDT) core. A structural frame was used to temporarily support the retaining wall until pluvial deposition was completed. A flexible rubber bag was placed inside the basement to contain the heavy fluid ($ZnCl_2$) used to simulate the effects of basement excavation. After pluvial deposition, the average sand densities in Tests CD51, CD68, SD69 and SS70 were 1486, 1542, 1546 and 1548 kg/m^3, corresponding to relative densities (D_r) of 51%, 68%, 69% and 70%, respectively. In Test CD51, the density of heavy fluid ($ZnCl_2$) placed inside basement was 1486 kg/m^3, while it was 1544 kg/m^3 in Tests CD68, SD69 and SS70.

Instrumentation

The vertical displacements of the tunnel along its longitudinal direction were monitored by the LVDTs together with extension rods installed at the crown (see Fig. 3a). For Tests CD51 and CD68 (in which the basement was excavated directly above the tunnel), three holes were made in the bottom of the rubber bags into which extension rods were inserted. Any gaps were sealed to prevent leakage of the heavy fluid.

Full-bridge strain gauges for temperature compensation were installed to measure bending moments induced in the tunnel not only along its transverse direction but also along its longitudinal direction. Semiconductor strain gauges (SSGs) were mounted on the outer surfaces of the tunnel to measure bending moments along the longitudinal tunnel direction. Along the tunnel crown and invert, 23 sets of SSGs were mounted at a spacing of 50 mm. Moreover, seven sets of SSGs were mounted along the springline at a spacing ranging from 60 to 80 mm. Conventional foil gauges (CFGs) were mounted on the outer and inner surfaces of the tunnel lining to measure bending moments along the transverse direction (i.e., S1 and S2). Sections S1 and S2 were located directly beneath and 100 mm (i.e., 0.33 L) away from the basement centre, respectively. In each monitoring section, eight sets of CFGs were mounted evenly at an interval of 45° around the circumference of the tunnel lining. Based on the measured bending moments and flexural stiffness of the model tunnel, induced strains in the tunnel along its longitudinal and transverse directions could be readily deduced by beam theory.

By installing four potentiometers inside tunnel lining, any increases or decreases in tunnel diameters could be measured in section S1 (i.e., directly beneath the basement centre). As shown in Figs. 3b and 3c, four linear potentiometers were fixed onto an aluminium plate connected to a supporting frame. This lightweight frame was mounted to the lining of existing tunnel using screws. The linear potentiometer is a variable resistor connected to three leads. Two leads are connected to both ends of the resistor, thus the resistance between them is fixed. Another lead is connected to a slider which can travel along the resistor. Accordingly, the resistance between the slider and the other two connections is varied. Any change in tunnel diameter is captured by the travel of the slider, which in turn alters the resistance of a potentiometer (Todd, 1975). By measuring the voltage between the slider and end of resistor, the travel distance of the slider (i.e., a change in tunnel diameter) can be calibrated and determined. Based on the analysis of measured data before the commencement of basement excavation, the accuracy of each potentiometer was estimated to be ±1 mm in prototype scale (Ng et al., 2013a). Two Druck PDCR-81 miniature pore pressure transducers were submerged in heavy fluid ($ZnCl_2$) to monitor the excavation depth. Moreover, one video camera was installed to record the entire test process.

Centrifuge testing procedure

Once the centrifuge model had been set up and following a final check, the model container was transferred to one of the centrifuge arms. Then the centrifuge was gradually spun up to 60 g. As soon as readings from the transducers had stabilised, the effects of basement excavation were simulated by draining away the heavy fluid ($ZnCl_2$) from the flexible rubber bag. Based on measurements from the pore pressure transducers submerged in the heavy fluid, three excavation stages were simulated in a sequential manner. The centrifuge was then spun down to 1 g until readings from all transducers again became stable.

THREE-DIMENSIONAL NUMERICAL ANALYSIS

To enhance the fundamental understanding of stress transfer and soil stiffness around the existing tunnel, three-dimensional numerical back-analyses of the four centrifuge tests were carried out using the software package ABAQUS (Hibbitt et al., 2008). A numerical parametric study was conducted to determine the effects of wall stiffness on the basement-tunnel interaction when the basement was constructed directly above the tunnel. For the case when the relative density of sand was 68%, five retaining systems (i.e., a sheet pile wall, 0.6, 0.96 and 1.5 m thick diaphragm walls and a rigid wall) were adopted to evaluate the effects of wall stiffness on the basement-tunnel interaction. Moreover, two final excavation depths of 9 and 15 m were considered. Correspondingly, the initial cover depths (C) of the tunnel were 2 D (12 m) and 3 D (18 m) respectively in the two scenarios. In all analyses, the clear distance between the tunnel crown and the formation level of the basement was kept at 0.5 D (3 m). The ratio between the wall penetration depth and the final excavation depth was taken as 0.5. A summary of all the numerical simulation parameters is given in Table 3.

Finite element mesh and boundary conditions

Figure 4 shows the three-dimensional finite element mesh used to back-analyse the centrifuge Test CD68. All dimensions in model scale were identical to those adopted in the centrifuge test. By conducting a numerical parametric study, the maximum difference of tunnel responses by adopting linear 8-node cubic (i.e., C3D8) and quadratic 20-node cubic elements (i.e., C3D20) to simulate soil stratum was within 6%. If C3D20 elements were used to replace C3D8 elements, the computational time was increased from 2 to 36 hours for each numerical run. In order to reduce computational time significantly, C3D8 elements were used to simulate the soil stratum in this study. According a numerical parametric study, the difference of tunnel responses by using 4-node shell elements (i.e., S4) and linear 8-node cubic elements (i.e., C3D8) to simulate sheet pile wall was less than 10%. Thus, the solid elements were selected to model both sheet pile wall and diaphragm wall in this study. Linear 8-node cubic elements (i.e., C3D8) were used to model the sand stratum and the retaining wall, while the tunnel lining was simulated with 4-node shell elements (i.e., S4). In total, the entire mesh consisted of 28064 solid elements (i.e., C3D8), 608 shell elements (i.e., S4) and

32896 nodes. By using a laptop computer with a CPU of 3.4 GHz and a ram memory of 8 GB, it took about two hours to finish a numerical run.

Soil movements were restrained in the x direction in the ABCD and EFGH planes, and in the y direction in the ABFE and CDHG planes. Moreover, soil movements in the x, y and z directions were restrained in the ADHE plane. In the numerical parametric study, the cover-to-tunnel diameter ratio (*C/D*) was varied from 2.0 to 3.0, corresponding to the final excavation depth of 9 and 15 m, respectively. For the cases with the final excavation depth of 15 m, the distance between the model wall and the outer boundary of the mesh was kept at least twice the final excavation depth to minimise boundary effects. By assuming a perfect contact of soil-structure interface, the computed maximum tunnel heave, longitudinal and transverse tensile strains were 11%, 12% and 6% smaller than those when interface friction angle was 20º (i.e., 2/3 φ'_c, frictional angle at the critical state). Thus, a perfect contact of soil-structure interface was assumed for simplicity.

Constitutive models and model parameters

Sand behaviours were described by a user-defined hypoplastic soil model which was incorporated in the software package ABAQUS using open-source implementation available for free download on the web (Gudehus et al., 2008). Hypoplastic constitutive models were capable of describing nonlinear response of soils. Various hypoplastic models have been developed in a number of studies (Kolymbas, 1991; Gudehus, 1996; Von Wolffersdorff, 1996; Wu et al., 1996; Mašín, 2012; Mašín, 2013; Mašín, 2014). The model proposed by Von Wolffersdorff (1996) was adopted in the present simulation to describe the behaviours of Toyoura sand. Hypoplasticity is a particular class of soil constitutive models characterised by the following rate formulation [1]:

[1] $$\overset{\circ}{\mathrm{T}} = f_s(\boldsymbol{L}: \mathbf{D} + f_d\mathbf{N}\|\mathbf{D}\|)$$

where $\boldsymbol{L}$ is a fourth-order tensor, $\mathbf{N}$ is a second-order tensor, $\mathbf{D}$ is rate of deformation f_s is a barotropy factor incorporating the dependency of the responses on mean stress level and f_d is a pyknotropy factor including the influence of relative density. In the hypoplastic formulation, the strain is not divided into elastic and plastic components.

The basic hypoplastic model requires eight material parameters (i.e., φ'_c, h_s, n, e_{d0}, e_{c0}, e_{i0}, α and β). Parameter φ'_c is angle of internal shearing resistance at critical state, which can be calibrated using the angle of repose test. Parameters h_s and n describe the slope and shape of limiting void ratio lines, i.e., isotropic normal compression line, critical state line and minimum void ratio line. Parameters e_{d0}, e_{c0} and e_{i0} are reference void ratios specifying positions of those three curves. e_{co} and e_{do} are related to e_{max} (maximum void ratio) and e_{min} (minimum void ratio) at zero stress level. By using results of oedometric test on loose sand, parameters h_s, n and e_{c0} can be calibrated. Parameters e_{d0} and e_{i0} can typically be estimated using empirical correlations. Parameters α and β control the dependency of peak friction angle and shear stiffness on relative density, respectively. Both of them can be estimated using triaxial shear test results. More information on model calibration can be found in Herle and Gudehus (1999).

By considering the intergranular strain concept, Niemunis and Herle (1997) enhanced the model for predictions of small strain stiffness and recent stress history. The modification requires five additional parameters, namely m_R, m_T, R, β_r and χ. Parameters m_R and m_T control very small strain shear modulus upon 180° and 90° change of strain path direction, respectively. The size of elastic range in the strain space is specified by parameter R. Parameters β_r and χ control the rate of stiffness degradation with strain. For details of calibration procedure for the intergranular strain concept, see Niemunis and Herle (1997).

Six parameters of Toyoura sand (φ'_c, h_s, n, e_{d0}, e_{c0} and e_{i0}) were obtained from Herle and Gudehus (1999), while triaxial test results reported by Maeda and Miura (1999) were used to calibrate parameters of α and β. According to the measured stiffness degradation curve in the small strain range of Toyoura sand reported by Yamashita et al. (2000), five parameters related to the intergranular strain were calibrated. Summary of all the parameters adopted in the present simulations was in Table 4. The same parameter set has already been successfully adopted in simulation of centrifuge tests by Ng et al. (2013a; 2013b). By using the equation proposed by Jáky (1944), the coefficient of at-rest earth pressure of soil (i.e., K_0 = 1-sin φ'_c) was estimated to be 0.5. The void ratio of soil was considered as a state variable in the hypoplastic model. For sand with different relative densities, the hypoplastic model can be used to evaluate the basement-tunnel interaction with a single set of material parameters. At 1 g conditions, void ratios of 0.78 and 0.72 (corresponding to relative sand density of 51% and 68%) were inputted as initial values in the back analyses of Tests CD51 and CD68, respectively.

A linearly elastic model was used to simulate the behaviours of the retaining wall and tunnel lining with Young's modulus ($E_{\text{aluminium}}$) of 70 GPa and a Poisson ratio (ν) of 0.2. The aluminium alloy used for the retaining wall and tunnel lining had a unit weight of 27 kN/m^3.

Numerical modelling procedure

The procedures adopted for numerical modelling were identical to those adopted for the centrifuge test. The exact simulation procedures are as follows:

1. Establish the initial boundary and stress conditions of soil at 1 g (i.e., gravitational acceleration) by assuming that the coefficient of at-rest earth pressure of soil (K_0) is 0.5. Then apply equivalent pressures on the wall and the formation level of the basement to simulate the existence of heavy fluid ($ZnCl_2$) inside the basement.

2. Increase the gravitational acceleration from 1 g to 60 g for the entire mesh (including soil, tunnel and retaining wall) in four steps. At each step, increase also the corresponding lateral and vertical fluid pressures applied on the wall and the formation level of the basement.
3. Decrease the lateral and vertical fluid pressures applied on the wall and the formation level of basement simultaneously (i.e., 3 steps in each run) to simulate the effects of basement excavation.

INTERPRETATION OF MEASURED AND COMPUTED RESULTS

All results are expressed in prototype scale unless stated otherwise.

Vertical displacement at the crown of the tunnel along its longitudinal direction

Figure 5 compares measured and computed vertical displacements at the crown of the tunnel along its longitudinal direction at the end of basement excavation. Positive and negative values denote tunnel heave and settlement, respectively. As the LVDT installed at the basement centre malfunctioned in Test CD68, tunnel heave was not obtained for that location.

In Tests CD51 and CD68 (in which the basement was excavated directly above the tunnel), heave was induced in the tunnel along its longitudinal direction due to vertical stress relief. Upon completion of basement excavation, the measured maximum tunnel heave at the basement centre was 0.09% H_e (final excavation depth) when the relative sand density was 51% (CD51). Moreover, the measured maximum tunnel heave in Test CD 68 (with a relative density of 68%) was 0.07% H_e at a distance of 0.2 L (basement length) from the basement centre. At this location, the tunnel heave in Test CD51 was only 5% larger than that in Test CD68. LTA (2000) recommended that the maximum tunnel movement be within 15 mm (i.e., 0.17% H_e). The maximum tunnel heave induced by basement excavation in this study is within the proposed allowable limit. The measured tunnel heaves gradually decreased with an increase in normalised distance from the basement centre. For the given model set-up, basement excavation exerted an influence on tunnel heave within 1.2 L (basement length) from the basement centre along the longitudinal direction of the tunnel. It was found that the measured and computed tunnel heaves in the longitudinal direction increased as the relative sand density decreased from 68% to 51%. Explanations are given in the next section.

During basement excavation, heave was induced in the soil beneath the basement, while settlement occurred behind the retaining wall. As shown in Figure 5, settlement was induced in the existing tunnel located at the side of the basement. For basements supported by sheet pile (SS70) and diaphragm walls (SD69), the maximum induced tunnel settlements were 0.018% H_e and 0.014% H_e, respectively. Note that the maximum tunnel settlement induced in Test SD 60 was less than 20% of the tunnel heave in Test CD68. Clearly the use of a 0.96 m thick diaphragm wall led to a 22% smaller maximum tunnel settlement than the use of a sheet pile wall. This is because a stiffer diaphragm wall can reduce the ground movements behind it and hence minimise tunnel settlement. The computed tunnel settlement also shows that tunnel settlement increased with decreasing wall stiffness. However, the profiles of the computed tunnel settlement were shallower and wider than the measured ones, probably because the stiffness anisotropy of soil was not properly captured by the constitutive model.

Vertical stress and mobilised shear stiffness of soil along the tunnel crown and invert

To fully understand the increase in tunnel heave with decreasing sand density (Tests CD51 and CD68), stress and stiffness of soil at the tunnel crown and invert along the longitudinal direction are compared. Figure 6a shows the computed changes in vertical stress at the tunnel crown and invert along the longitudinal direction. Positive and negative values denote increases and decreases in stress acting on the tunnel lining, respectively.

Along the tunnel crown, the vertical stress of soil beneath the basement was significantly reduced due to the removal of soil simulated by decreasing the lateral and vertical pressures applied on the wall and the formation level of the basement. On the contrary, an increase in vertical stress of up to 68 kPa was observed in the soil underneath the bottom of retaining wall. As basement excavation proceeded, the entire tunnel moved upward as shown in Fig. 5. Moreover, ground settlement was induced behind the retaining wall generating downward friction. Due to a combination of upward tunnel movement and downward wall-soil friction, stress in the soil between the retaining wall and the model tunnel increased accordingly. At a distance of 0.2 *L* (basement length) to 0.7 *L* behind the retaining wall, a slight increase in soil stress (less than 5 kPa) was observed at the crown. On the other hand, the vertical stress of soil beneath the tunnel invert decreased along the longitudinal direction of the tunnel, even at a distance of 1.0 *L* behind the retaining wall. This is because the existing tunnel moved upward during basement excavation resulting in stress reduction at the invert.

At the end of basement excavation, the maximum changes in vertical stress at the tunnel crown and invert exceeded the allowable limit (i.e., ±20 kPa) set by BD (2009). Thus, the structural integrity of the existing tunnel should be reviewed based on changes in the loading condition acting on the lining. Cracks or even collapse may be induced in the tunnel, depending on the magnitude of stress changes surrounding the lining. Along the tunnel crown, stress changes in the soil behind the retaining wall stayed within the allowable limit. However, stress changes in the soil at the tunnel invert exceeded the allowable limit at a distance of less than 0.4 *L* behind the retaining wall. Note that the maximum vertical stress relief at the tunnel crown was about five times that at the invert. The large reduction in stress makes it imperative to review the structural integrity of the existing tunnel, especially at the crown. Although the relative sand density in Test CD51 was 25% smaller than that in Test CD68, vertical stress relief at the tunnel crown and invert in looser soil was about 1% smaller than that in denser soil as expected.

Figure 6b shows the relationships between the mobilised secant shear stiffness of soil at the tunnel crown and the normalised distance from the basement centreline. For clarity, the mobilised shear stiffness of soil at the tunnel invert is not shown in this figure. By taking the deviatoric stress (q) and shear strain (ε_s) from numerical analyses, the mobilised secant shear stiffness ($q/3\varepsilon_s$) of soil at a given stage can be obtained. After increasing g-level to 60 g, the mobilised secant shear stiffness of soil located directly underneath the diaphragm wall was much larger than that in other regions. This is because compression of the soil between the tunnel and the retaining wall resulted in higher soil stress in this region. Upon completion of basement excavation, the mobilised secant shear stiffness of soil beneath the basement was significantly reduced due to the removal of vertical stress at the tunnel crown (see Fig. 6a) and accumulative shear strain in soil. Although stress of soil located underneath the bottom of retaining wall increased as excavation proceeded, the stiffness of soil at this location was reduced. This is because basement excavation induced further compression of soil underneath the wall causing significant stiffness degradation. Due to stress relief along the tunnel invert (see Fig. 6a), the mobilised shear stiffness of soil along the invert decreased during basement excavation.

Along the tunnel crown, the mobilised secant shear stiffness of soil beneath the basement in looser sand (CD51) was 35-42% smaller than that in denser sand (CD68) upon completion of increasing g-level and basement excavation. Moreover, the mobilised shear stiffness of soil at the tunnel invert in Test CD51 was 33% smaller than that in Test CD68. However, the differences in stress changes at the tunnel crown and invert were negligible when relative sand density varied from 68% to 51% (see Fig. 6a). Thus, an increase in tunnel heave with decreasing sand density was observed. As the sand density decreased from 68% to 51%, the maximum heave in tunnel increased by about 5%. This indicates that excavation-induced maximum tunnel heave was not sensitive to a change in sand density from 68% to 51% even though the mobilised shear stiffness of soil was significantly reduced by more than 30% at the crown and invert.

Displacement vectors of soil around the existing tunnel located at the side of the basement

To improve the understanding of the variation in tunnel settlement with wall stiffness, displacement vectors of soil around the tunnel located at the side of the basement were computed. Figure 7 shows the computed displacement vectors of soil around the existing tunnel and the basement upon completion of excavation. As expected, heave was induced in the soil beneath the basement due to vertical stress relief. Because the forces on the excavated side and the retained side were unbalanced, the soil behind the retaining wall moved downward toward the basement. As shown in the figure, soil settlement was induced around the existing tunnel except at the right springline and the right knee resulting in tunnel settlement accordingly. In addition, the soil surrounding the existing tunnel also moved toward the basement, implying that the tunnel also bent toward the basement during excavation.

The computed ground movement behind the retaining wall was much more significant when a sheet pile wall was adopted instead of a 0.96 m thick diaphragm wall. Moreover, induced heave in the soil beneath the basement increased as the flexural stiffness of the retaining wall reduced. This is because much more soil was squeezed into the basement and larger inward wall movement was induced when a sheet pile was used. As the lateral wall movement of the sheet pile wall was much larger than that of the diaphragm wall, a much larger lateral soil movement was observed near the excavated side of retaining wall with a smaller flexural stiffness. It was also found that soil settlement around the existing tunnel increased with a reduction in the flexural stiffness of the retaining wall. Correspondingly, a trend of increasing tunnel settlement with a decrease in wall stiffness could be observed (see Fig. 5).

The lateral and vertical movements of soil above the formation level and behind retaining wall decreased significantly when the retaining wall increased in stiffness. For a tunnel located at any of those locations, adopting a stiff retaining wall should be an effective way to alleviate the adverse effects of basement excavation.

Changes in tunnel diameter

Figure 8 compares measured and computed changes in tunnel diameter with the unloading ratio. All the results were taken at section S1which was located directly underneath basement (see Fig. 2a). The unloading ratio is defined as the excavation depth (H) to the initial tunnel cover depth (C). Positive and negative values denote elongation and compression of the tunnel, respectively.

Due to a reduction in vertical stress accompanied by a smaller horizontal stress relief around the tunnel lining, vertical elongation and horizontal compression were induced in the tunnel located beneath the basement centre (i.e., section S1 as shown in Fig. 2a). The vertical elongation and horizontal compression of the tunnel increased with the unloading ratio. Once basement excavation had ended, the maximum vertical elongation (ΔD_V) and horizontal compression (ΔD_H) of the tunnel in Test CD51 were measured to be 0.16% D (tunnel diameter) and 0.20% D, respectively. Moreover, a maximum vertical elongation of 0.13% D and horizontal compression of 0.16% D were measured in the tunnel in Test CD68. BTS (2000) recommended that the maximum distortion of a tunnel ($(\Delta D_V+\Delta D_H)/D$) was within

2%. The maximum distortion induced in the existing tunnel (i.e., 0.36% D) in this study is within the recommended limit.

At basement centre (i.e., section S1), the measured maximum vertical elongation and horizontal compression of the tunnel increased by 23% and 25%, respectively, as the relative sand density decreased from 68% to 51%. Computed results also show that the magnitude of tunnel deformation increased with a reduction in the sand density. However, the computed changes in tunnel diameters were 32% to 48% smaller than the measured ones.

To explain the variations in tunnel diameters with sand density, the mobilised secant shear stiffness ($G = q/3\varepsilon_s$) of soil along the transverse direction of the tunnel was computed at section S1 (i.e., underneath basement centre). Figure 9 shows the normalised secant shear modulus of soil along the transverse direction of the tunnel. In total, the secant shear modulus of soil at sixteen points was obtained. At each location, the secant modulus of soil with a relative density of 51% (i.e., G_{CD51}) was normalised by that in a sand with a relative density of 68% (i.e., G_{CD68}). Due to a smaller void ratio in a denser sand, the normalised secant shear modulus of soil (G_{CD51}/G_{CD68}) along the transverse tunnel direction was about 0.65 after the g-level was increased to 60 g. Upon completion of simulating basement excavation, the normalised shear modulus of soil above the tunnel springline was decreased to 0.58, but that of soil below the tunnel springline was increased to 0.73. After increasing g-level and basement excavation, the computed soil stiffness around the transverse tunnel direction in a looser sand (i.e., CD51) was found to be much smaller than that in a denser sand (i.e., CD68). This implies that a tunnel buried in a looser sand is less resistant to vertical elongation when it was subjected to stress relief. Moreover, a larger inward wall movement is induced in a looser sand (i.e., CD51) due to a smaller stiffness of soil around the tunnel. Thus, basement excavation in a looser sand caused a larger horizontal compression in a tunnel. Because of these two factors, larger vertical elongations are induced in the tunnel accordingly.

Correspondingly, a larger horizontal compression is induced in a tunnel buried in a looser sand.

Induced strain in the tunnel along its transverse direction

Figure 10 shows the measured and computed strains at the outer surface of the tunnel lining along the transverse direction of the tunnel. All the strains presented in this figure are incremental, i.e., due to basement excavation only. Positive and negative values denote tensile and compressive strains, respectively. By taking bending moment of the aluminium alloy tube from centrifuge tests and numerical analyses, strain of an unreinforced concrete tunnel with equivalent flexural stiffness (i.e., with Young's modulus of 35 GPa and thickness of 230 mm) was calculated by using beam theory. All the results were taken at two sections of existing tunnel, i.e., directly beneath (section S1) and 0.33 *L* (section S2) away from the basement centre, respectively.

Due to symmetrical stress relief around the tunnel lining, the profiles of measured and computed strains were symmetrical for the tunnel located directly beneath and 0.33 *L* away from basement centre (i.e., sections S1 and S2) as expected. Tensile strains were induced at the outer surface of the tunnel crown, shoulder, knee and invert, corresponding to elongation of the tunnel at those locations. On the other hand, compressive strain was measured and computed at the outer surface of the tunnel springline, corresponding to compression of the tunnel at that particular location. Variations in strains in the tunnel along its transverse direction were consistent with changes in tunnel diameters measured by the potentiometers (see Fig. 8). Upon completion of basement excavation, the maximum tensile strain of 132 $\mu\varepsilon$ in the tunnel along its transverse direction was measured beneath the basement centre (i.e., section S1). According to ACI224R (2001), the ultimate tensile strain of unreinforced concrete is 150 $\mu\varepsilon$. So if the tensile strain in the existing tunnel is above 18 $\mu\varepsilon$ even before basement excavation, the tunnel could crack. Compared with the strain at section S1 (i.e., beneath the basement centre), the strain at section S2 (i.e., 0.33 L away from the basement centre) was reduced by 20-30%.

Both measured and computed maximum tensile strain at the tunnel crown was much larger than that at the invert. This is because the tunnel crown experienced a much larger stress relief than the invert (see Fig. 6a). At a given tensile strain in the tunnel along its transverse direction, the crown was more vulnerable to cracking than the invert. For tunnel located directly underneath basement centre (i.e., section S1), the measured maximum tensile strains in the tunnel along its transverse direction were 132 and 110 $\mu\varepsilon$, respectively, in Tests CD51 and CD68. This indicates that the measured maximum tensile strain in the tunnel increased by 20% when the relative sand density decreased from 68% (CD68) to 51% (CD51). The computed maximum tensile strain also increased with a reduction in sand density. It is consistent with variations in tunnel diameters with the relative sand density as shown in Fig. 8. This is because a looser soil is less stiff around a tunnel and hence the inward wall movement would be larger.

In the cases of SD69 and SS70 (in which the basement was excavated at the side of the tunnel), both measured and computed strains showed that the shape of the tunnel was clearly distorted due to unsymmetrical stress relief and shearing around it. At both sections S1 and S2, the maximum tensile strain was measured and computed in the right shoulder (close to the basement) of the tunnel. Upon completion of basement excavation, the maximum tensile strains in the tunnel located at basement centre (i.e., section S1) were measured to be 34 and 69 $\mu\varepsilon$ respectively in Tests SD69 and SS70. Under the same sand density and wall stiffness, the maximum transverse tensile strain of tunnel in Test SD60 was only about 31% of that in Test CD68. At section S1, the measured maximum tensile strain in the tunnel located at the side of the basement (i.e., 69 $\mu\varepsilon$ in Test SS70) was only 52% of that in the tunnel located directly beneath the basement (i.e., 132 με in Test CD51). It is obvious that the maximum tensile strain in the tunnel along its transverse direction was reduced by more than 50% when a diaphragm wall was adopted to replace a sheet pile wall. As expected, the sheet pile wall moved inward to a larger extent causing a greater stress reduction around the tunnel lining. A discussion on the reduced normal stress acting on the tunnel lining is given in the next section.

According to the numerical parametric study by Shi et al. (2015), the basement-tunnel interaction at basement centre could be simplified as a plane strain condition when the excavation length (i.e., L) along the longitudinal tunnel direction reached 9 H_e (excavation depth). For the short excavation (i.e., L/H_e = 2.0) reported in this study, induced tunnel heave and transverse tensile strain at basement centre were less than 30% of that in a long and narrow excavation (i.e., L/H_e = 9.0). It implies that corner stiffening in a short excavation significantly reduced tunnel heave and tensile strain by basement excavation.

Reduced normal stress acting on the tunnel lining along its transverse direction

Figure 11 shows the reduction in normal stress acting on the tunnel lining along its transverse direction as a result of basement excavation. Excavation induced reduction in normal stress around tunnel lining is computed in section S1 which is located beneath basement centre For a tunnel located beneath the basement centre (CD51 and CD68), the profiles of reduced normal stress acting on the tunnel lining were symmetrical as expected. Stress relief along the vertical direction was larger than that along the horizontal direction. Thus, the existing tunnel was vertically elongated and horizontally compressed (see Figs. 8 & 10). Accordingly, tensile strain was induced at the outer surface of the tunnel crown and invert, while compressive strain was observed at the outer surface of the tunnel springline. Note that the reduction in normal stress at the tunnel crown was about five times larger than that at the invert. Correspondingly, a much larger tensile strain was induced at the crown than at the invert (see Fig. 10). As expected, the extent of normal stress reduction around the tunnel lining changed little (less than 1%) as the relative sand density decreased from 68% (CD68) to 51% (CD51). However, the maximum transverse tensile strain at the tunnel crown in Test CD51 was 20% larger than that in Test CD68. This is because a looser soil is less stiff around the tunnel (see Fig. 9) and hence the wall moved inward to a greater extent. Thus, a stiffer retaining wall can be used to reduce excavation-induced tensile strain in the tunnel along its transverse direction.

For a tunnel located at the side of the basement, the reduction in normal stress acting on the tunnel lining was clearly asymmetrical. The stress relief at the tunnel right shoulder and springline, which are closer to the basement, was much larger than that at other locations. Correspondingly, the tunnel lining was elongated toward the basement as shown in Fig. 10. Note that a much larger stress reduction occurred around the tunnel lining when the sheet pile wall (SS70), as opposed to the diaphragm wall (SD69), was adopted. Due to an increase in stress relief around the tunnel lining with decreasing wall stiffness, a much larger transverse tensile strain was observed in Test SS70 than in Test SD69 (see Fig. 10).

For a tunnel located beneath the basement centre (CD51 and CD68), the reduction in normal stress around the tunnel lining exceeded the allowable limit (of 20 kPa according to BD (2009)). Because of large stress changes around existing tunnel, attention should be paid to the integrity of existing tunnel lining. For a tunnel located at the side of the basement (SD69 and SS70), however, only the section of the tunnel lining closest to the basement experienced stress changes larger than the allowable limit. Note that the maximum reduction in normal stress in the latter tunnel was 43% of that in the former tunnel. This is consistent with the measured tensile strain in tunnel (i.e., located outside the basement) along its transverse direction as shown in Fig. 10.

Induced strain in the tunnel along its longitudinal direction

Figure 12 shows the measured and computed strains in the tunnel along its longitudinal direction. Positive and negative values denote tensile and compressive strains at the tunnel crown, corresponding to hogging and sagging moments, respectively.

For a tunnel located directly beneath the basement centre (CD51 and CD68), the profiles of measured strains at the tunnel crown along the longitudinal direction were symmetrical with respect to the basement centre as expected. This implies that uniformity was achieved in the preparation of sand samples. Due to differential tunnel heave as shown in Fig. 5, hogging and sagging moments were induced at the basement centre and other locations. By inspecting the strains measured at the tunnel crown along the longitudinal direction of the tunnel, the inflection point where strain is equal to zero can be identified. In these two tests, the inflection point, where the shear force was at a maximum, was about 0.8 L (i.e., basement length) away from the basement centre.

A reasonably good agreement between measured and computed results was obtained except for induced strain at the basement centre. Both measured and computed strains in the tunnel along its longitudinal direction increased due to a reduction in sand density. Upon completion of basement excavation, the measured maximum strains in the hogging and sagging regions increased by 15% and 13%, respectively, as the relative sand density decreased from 68% (CD68) to 51% (CD51). This is consistent with the finding shown in Fig. 5 that longitudinal tunnel heave increased as soil density was reduced. This is because the mobilised shear stiffness of soil at the tunnel crown and invert was significantly reduced as sand density decreased from 68% to 51%, while differences in soil stress relief at those locations were negligible (see Fig. 6).

For clarity, induced strain in the tunnel located at the side of the basement is not shown in Figure 12. Due to excavation-induced differential settlement of that tunnel (see Fig. 5), sagging and hogging moments were induced at the basement centre and other locations, respectively. Once basement excavation had ended, the maximum tensile strains at tunnel crown were measured to be 12 and 18 με, respectively, when the tunnel was retained by the diaphragm wall (SD69) and when it was retained by the sheet pile wall (SS70). In addition, the measured maximum tensile strains at the tunnel springline in Tests SD69 and SS70 were 5 and 12 με, respectively. Therefore, using a diaphragm wall (SD69) instead of a sheet pile wall (SS70) reduced the measured maximum tensile strains in the tunnel along its longitudinal direction by up to 58%. This is because a stiffer wall can reduce the ground movements behind it and hence minimise tensile strain in a tunnel. Moreover, the maximum longitudinal tensile strain of tunnel in Test SD60 was only about 18% of that in Test CD68.

For a tunnel located at the side of the basement, the maximum strains in the longitudinal and transverse directions were only 23% and 53% of the corresponding values for a tunnel located directly beneath the basement. Moreover, the maximum movement of the former tunnel was measured to be just 21% of that of the latter tunnel. By using a sheet pile wall to replace a diaphragm wall, excavation induced responses of tunnel at a side of basement (i.e., SS70) were still small. Thus, it is decided that the influence of sand density on tunnel responses was not considered for this case. In this paper, the numerical parametric study only focused on the influence of wall stiffness on the responses of tunnel when it was located directly underneath basement centre.

Effects of wall stiffness on three-dimensional tensile strains induced in the tunnel

Figure 13 shows the relationships between wall stiffness and excavation-induced three-dimensional tensile strains in the tunnel located directly beneath the basement centre. All the strains plotted in this figure are due to overlying basement excavation only. A retaining wall with a flexural stiffness (E_wI_w) of 2.58×10^5 MN·m in prototype is equivalent to a 4.5 m thick diaphragm wall assuming Young's modulus of concrete of 35 GPa. Since the induced maximum lateral movement of the wall was less than 0.1 mm in prototype, the retaining wall can be considered as a rigid wall. In this case, the induced heave and tensile strain in the tunnel were attributed to vertical stress relief and soil movement behind the retaining wall rather than inward wall movement.

As shown in Figure 13a, the maximum tensile strain in the tunnel along its longitudinal direction increased slightly when wall stiffness increased from 80 (sheet pile wall) to 9.84×10^3 MN·m (1.5 m diaphragm wall) in prototype. However, tensile strain in the tunnel did not change much when wall stiffness was further increased to 2.58×10^5 MN·m (rigid wall). The maximum tensile strain in the tunnel along its longitudinal direction was computed to have varied by up to 15% when a rigid wall was adopted instead of a sheet pile wall. This implies that the maximum tensile strain induced in the tunnel along its longitudinal direction is insensitive to the flexural stiffness of retaining wall, given the model geometry used.

In contrast, induced maximum tensile strain at the crown of the tunnel along its transverse direction was significantly affected by the flexural stiffness of the retaining wall as shown in Figure 13b. The maximum tensile strain was reduced by more than 40% when a 1.5 m thick diaphragm wall was adopted instead of a sheet pile wall. Another 10% reduction in the maximum tensile strain was made by further increasing the wall stiffness to 2.58×10^5 MN·m (i.e., rigid wall). This is because inward wall movement was significantly reduced for the stiff diaphragm wall and so the tensile strain in the tunnel was minimised. Adopting a stiff retaining wall is therefore an effective way to reduce the maximum tensile strain induced in the tunnel along its transverse direction by basement excavation.

The maximum tensile strain in the tunnel along its longitudinal direction differed by less than 15% when a rigid wall was adopted as opposed to a sheet pile wall. However, the maximum tensile strain at the tunnel crown along its transverse direction was reduced by more than 50%. This is because a tunnel has a much smaller flexural stiffness in the transverse direction than in the longitudinal direction.

SUMMARY AND CONCLUSIONS

A series of three-dimensional centrifuge tests were designed and carried out to investigate the effects of sand density and retaining wall stiffness on responses of a tunnel to basement excavation. Three-dimensional numerical back-analyses and a parametric study were also conducted to improve the fundamental understanding of these effects on the basement-tunnel interaction. Based on the measured and computed results, the following conclusions may be drawn:

(1) For the tunnel located directly beneath the basement, excavation-induced heave and strain along its longitudinal direction were not sensitive to a change in sand density from 68% to 51%, even though the mobilised shear stiffness of soil was significantly reduced by more than 30% at the crown and invert.

(2) Due to a reduction in vertical stress accompanied by a relatively smaller horizontal stress relief around the tunnel lining, vertical elongation and horizontal compression were induced in the tunnel located directly beneath the basement centre. The elongation and maximum tensile strain induced in the tunnel along its transverse direction increased by more than 20% as the relative sand density decreased from 68% to 51%. This is because a looser soil is less stiff around the tunnel resulting in a larger inward wall movement. Tunnel responses along the transverse direction are more sensitive to density variations because a tunnel has a much smaller stiffness along this direction than along the longitudinal direction.

(3) For the tunnel located at the side of the basement, the measured maximum settlement and strain along its longitudinal direction were reduced by up to 22% and 58%,

respectively, when a diaphragm wall was adopted instead of a sheet pile wall. This is because a stiffer diaphragm wall can significantly reduce the ground movements behind it and hence minimise the longitudinal settlement of the tunnel. Thus, a stiff wall can be used to alleviate basement excavation induced adverse effects on existing tunnel.

(4) Because of unsymmetrical stress relief and shearing, distortion was induced in the transverse direction of the existing tunnel located at the side of the basement. When the tunnel was placed behind a sheet pile wall, the maximum tensile strain in the tunnel along its transverse direction was twice as large as that when the tunnel was placed behind a diaphragm wall. This is because the normal stress relief around the tunnel was much larger in the former case. Thus, a stiffer retaining wall can be used to alleviate excavation-induced tensile strain in the tunnel along its transverse direction.

(5) Under the same soil density and wall stiffness, basement excavation induced maximum movement and tensile strains in the tunnel located at a side of basement were about 30% of the corresponding values measured in the tunnel located directly beneath basement centre. For given the model geometry in this study, it is thus suggested to construct a basement at a side of tunnel rather than above it.

(6) For the tunnel located directly beneath basement centre, dimensionless calculation charts were developed to estimate the influence of wall stiffness on the maximum tensile strain of tunnel along its longitudinal and transverse directions. Three-dimensional tensile strains induced in the tunnel by basement excavation were observed in the calculation charts. The maximum tensile strain induced in the tunnel along its longitudinal direction was insensitive to wall stiffness while a stiffer retaining wall significantly reduced the maximum tensile strain induced in the transverse direction. This is because a tunnel has a much smaller flexural stiffness along its transverse direction than along its longitudinal direction.

ACKNOWLEDGEMENTS

The authors would like to acknowledge the financial supports provided by the Research Grants Council of the HKSAR (General Research Fund project No. 617511), the Program for Changjiang Scholars and Innovative Research Team in University (Grant No. IRT1125) and the 111 Project (Grant No. B13024).

REFERENCES

American Concrete Institute. 2001. Control of cracking in concrete structures (ACI 224R-01). American Concrete Institute, Mich., USA.

Atkinson, J. H., Richardson, D., and Stallebrass, S. E. 1990. Effect of recent stress history on the stiffness of overconsolidated soil. Géotechnique, 40 (4): 531-540.

Buildings Department. 2009. Practice note for authorized persons APP-24. Technical notes for guidance in assessing the effects of civil engineering construction/building development on railway structures and operations. Building department of the government of HKSAR (BD).

Bolton, M. D., and Powrie, W. 1988. Behavior of diaphragm walls: retaining walls prior to collapse. Géotechnique, 37 (3): 335-353.

BTS. 2000. Specification for tunnelling. British Tunnelling Society (BTS). Thomas Telford, London.

Burford, D. 1988. Heave of tunnels beneath the Shell Centre, London, 1959-1986. Géotechnique, 38 (1): 135-137.

Chang, C.-T., Sun, C.-W., Duann, S.W., and Hwang, R.N. 2001. Response of a Taipei Rapid Transit System (TRTS) tunnel to adjacent excavation. Tunnelling and Underground Space Technology, 16 (3): 151-158.

Doležalová, M. 2001. Tunnel complex unloaded by a deep excavation. Computer and Geotechnics, 28 (6): 469-493.

Gudehus, G. 1996. A comprehensive constitutive equation for granular materials. Soils and Foundations, 36(1): 1-12.

Gudehus, G., Amorosi, A., Gens, A., Herle, I., Kolymbas, D., Mašín, D., Muir Wood, D., Niemunis, A., Nova, R., Pastor, M., Tamagnini, C., Viggiani, G. 2008. The soilmodels.info project. International Journal for Numerical and Analytical Methods in Geomechanics, 32(12): 1571-1572.

Herle, I., and Gudehus, G. 1999. Determination of parameters of a hypoplastic constitutive model from properties of grain assemblies. Mechanics of Cohesive-frictional Materials, 4 (5): 461-486.

Hibbitt, Karlsson and Sorensen Inc. 2008. ABAQUS User’s Manual, version 6.8.2.

Hsieh, P.-G., and Ou, C.-Y. 1998. Shape of ground surface settlement profiles caused by excavation. Canadian Geotechnical Journal, 35 (6): 1004-1017.

Hu, Z. F., Yue, Z. Q., Zhou, J., and Tham, L. G. 2003. Design and construction of a deep excavation in soft clay adjacent to the shanghai metro tunnels. Canadian Geotechnical Journal, 40(5): 933-948.

Huang, X., Huang H.W., and Zhang, D.M. 2012. Centrifuge modeling of deep excavation over existing tunnels. Proceedings of the ICE-Geotechnical Engineering (in press).

Huang, X., Schweiger, H.F., and Huang. H.W. 2013. Influence of deep excavations on nearby existing tunnels. International Journal of Geomechanics, ASCE, 13 (2): 170-180.

Ishihara, K. 1993. Liquefaction and flow failure during earthquakes. Géotechnique, 43(3): 351-415.

Jáky, J. 1944. The coefficient of earth pressure at rest. Journal for the Society of Hungarian Architects and Engineers, 7: 355-358.

Karki, R. 2006. Effects of deep excavations on circular tunnels in fine-grained soils. M.Ph. thesis, University of Saskatchewan, Saskatoon, SK, Canada.

Kolymbas, D. 1991. An outline of hypoplasticity. Archive of Applied Mechanics, 61: 143-151.

Leung, C. F., Chow, Y. K., and Shen, R. F. 2001. Behavior of pile subject to excavation-induced soil movement. Journal of Geotechnical and Geoenvironmental, ASCE, 126

(11): 947-954.

Leung, C. F., Lim, J. K., Shen, R. F., and Chow, Y. K. 2003. Behavior of pile groups subject to excavation-induced soil movement. Journal of Geotechnical and Geoenvironmental, ASCE, 129 (1): 58-65.

Liu, H. L., Li, P., and Liu, J. Y. 2011. Numerical investigation of underlying tunnel heave during a new tunnel construction. Tunnelling and Underground Space Technology, 26(2): 276-283.

Lo, K.Y., and Ramsay, J.A. 1991. The effect of construction on existing subway tunnels-a case study from Toronto. Tunnels and Deep Space, 6(3): 287-297.

Long, M. 2001. Database for retaining wall and ground movements due to deep excavation. Journal of Geotechnical and Geoenvironmental Engineering, ASCE, 127(3): 203-224.

LTA. 2000. Code of practice for railway protection. Development & Building Control Department, Land Transport Authority (LTA), Singapore.

Maeda, K., and Miura, K. 1999. Relative density of dependency of mechanical properties of sands. Soils and Foundations, 39 (1): 69-79.

Mašín, D. 2012. Hypoplastic Cam-clay model. Géotechnique, 62 (6): 549-553.

Mašín, D. 2013. Clay hypoplasticity with explicitly defined asymptotic states. Acta Geotechnica, 8 (5): 481-496.

Mašín, D. 2014. Clay hypoplasticity model including stiffness anisotropy. Géotechnique, 64 (3): 232-238.

Meguid, M.A., Rowe, R.K., and Lo, K.Y. 2002. 3D effects of surface construction over existing subway tunnels. International Journal of Geomechanics, ASCE, 2 (4): 447-469.

Mohamad, H., Bennett, P. J., Soga K., Mair R. J., and Bowers, K. 2010. Behaviour of an old masonry tunnel due to tunnelling-induced ground settlement. Géotechnique, 60 (12): 927–938.

Ng, C.W.W., Boonyarak, T., and Mašín, D. 2013a. Three-dimensional centrifuge and numerical modeling of the interaction between perpendicularly crossing tunnels. Canadian Geotechnical Journal, 50 (9): 935-946.

Ng, C.W.W, Shi, J., and Hong, Y. 2013b. Three-dimensional centrifuge modelling of basement excavation effects on an existing tunnel in dry sand. Canadian Geotechnical Journal, 50 (8): 874-888.

Ng, C.W.W., Van Laak, P., Tang, W.H., Li, X.S., and Zhang, L.M. 2001. The Hong Kong geotechnical centrifuge. Proc. 3rd Int. Conf. Soft Soil Engineering, 225-230.

Ng, C.W.W., Van Laak, P.A., Zhang, L.M., Tang, W.H., Zong, G.H., Wang, Z.L., Xu, G.M., and Liu, S.H. 2002. Development of a four-axis robotic manipulator for centrifuge modeling at HKUST. Proc. Int. Conf. Physical Modelling in Geotechnics, St. John's Newfoundland, Canada, 71-76.

Niemunis, A. and Herle, I. 1997. Hypoplastic model for cohensionless soils with elastic strain range. Mechanics of Cohesive-frictional Material, 2: 279-299.

Peck, R.B. 1969. Deep excavations and tunneling in soft ground. Proceedings of the 7th International Conference on Soil Mechanics and Foundation Engineering, Sociedad Mexicana de Mecanica de Suelos, A.C., Mexico City, pp.225-290.

Powrie, W., Pantelidou, H., and Stallebrass, S. E. 1998. Soil stiffness in stress paths relevant to diaphragm walls in clay. Géotechnique, 48 (4): 483-494.

Sharma, J.S., Hefny, A.M., Zhao, J., and Chan, C.W. 2001. Effect of large excavation on displacement of adjacent MRT tunnels. Tunnelling and Underground Space Technology, 16 (2): 93-98.

Shi, J., Ng, C. W. W., and Chen, Y. H. 2015. Three-dimensional numerical parametric study of the influence of basement excavation on existing tunnel. Computers and Geotechnics 63: 146-158.

Sun, Y., Xu, Y.-S., Shen, S.-L., and Sun, W.-J. 2012. Field performance of underground structures during shield tunnel construction. Tunnelling and Underground Space Technology, 28 (1): 272-277.

Taylor, R.N. 1995. Geotechnical centrifuge technology. Blackie Academic and Professional, London.

Todd, C. D. 1975. The potentiometer handbook. McGraw-Hill, New York.

Von Wolffersdorff, P. A. 1996. A hypoplastic relationship for granular material with a predefined limit state surface. Mechanics of Cohesive-frictional Material, 1: 251-271.

Wang, J. H., Xu, Z. H., and Wang, W. D. 2010. Wall and ground movements due to deep excavations in Shanghai soft soil. Journal of Geotechnical and Geoenvironmental Engineering, ASCE, 136 (7): 985-994.

Wang, Z., Wang, L., Li, L., and Wang, J. 2014. Failure mechanism of tunnel lining joints and bolts with uneven longitudinal ground settlement. Tunnelling and Underground Space Technology, 40: 300-308.

Wu, W., Bauer, E., and Kolymbas, D. 1996. Hypoplastic constitutive model with critical state for granular materials. Mechanics of Materials, 23 (1): 45-69.

Yamashita, S., Jamiolkowski, M., and Lo Presti, D.C.F. 2000. Stiffness nonlinearity of three sands. Journal of Geotechnical and Geoenvironmental Engineering, ASCE, 126 (10): 929-938.

Zheng, G., Peng, S. Y., Ng, C. W. W., and Diao, Y. 2012. Excavation effects on pile behaviour and capacity. Canadian Geotechnical Journal, 49 (12): 1347-1356.

Zheng, G., and Wei, S.W. 2008. Numerical analysis of influence of overlying pit excavation on existing tunnels. Journal of Central South University of Technology, 15(s2): 69-75.

List of captions

Tables

Table 1. Relevant scaling laws (Taylor, 1995; Ng et al., 2013b)

Table 2. Centrifuge test program

Table 3. Numerical analysis program

Table 4. Summary of material parameters adopted for finite element analysis (Ng et al., 2013a; 2013b)

Figures

Fig. 1. Plan view of the centrifuge model

Fig. 2. Elevation views of the centrifuge model: (a) section A-A and (b) section B-B

Fig. 3. (a) Types and locations of instruments installed on the existing tunnel; (b) Transverse section view; (c) Longitudinal section view (Unit: mm. All dimensions in model scale)

Fig. 4. (a) The three-dimensional finite element mesh adopted in this study; (b) Intersection of the tunnel and the retaining wall in detail (Unit: mm. All dimensions in model scale)

Fig. 5. Normalised vertical displacement of the tunnel along its longitudinal direction

Fig. 6. Computed soil responses around the tunnel: (a) changes in vertical stress at the crown and invert; (b) mobilised secant shear stiffness of soil at the crown

Fig. 7. Computed soil displacement vectors around the basement and the tunnel

Fig. 8. Elongation and compression of the tunnel located beneath the basement centre

Fig. 9. Mobilised secant shear stiffness of soil along the transverse direction of the tunnel in section S1

Fig. 10. Induced strain at the outer surface of the tunnel along its transverse direction

Fig. 11. Reduced normal stress acting on the tunnel lining in section S1 (Unit: kPa)

Fig. 12. Effects of sand density on induced strain in the tunnel along its longitudinal direction

Fig. 13. Effects of wall stiffness on three-dimensional tensile strains induced in the tunnel by basement excavation

Tables

Table 1. Relevant scaling laws (Taylor, 1995; Ng et al., 2013b)

Parameter	Scaling law (model/prototype)
Gravity (m/s^2)	N
Length (m)	1/N
Strain	1
Stress (kPa)	1
Density (kg/m^3)	1
Unit weight (N/m^3)	N
Bending moment (N·m)	1/N^3
Bending moment per meter run (N·m/m)	1/N^2
Flexural stiffness (N·m^2)	1/N^4
Flexural stiffness per meter run (N·m^2/m)	1/N^3

Table 2. Centrifuge test program

ID	Relative sand density (D_r)	Retaining wall type	Remark
CD51	51%	DW	Basement constructed directly above the existing tunnel
CD68	68%	DW	
SD69	69%	DW	Basement constructed at the side of the existing tunnel
SS70	70%	SW	

DW: diaphragm wall; SW: sheet pile wall

Table 3. Numerical analysis program

Tunnel location	Relative sand density (D_r)	Retaining wall type	Cover-to-diameter ratio (C/D)	Final excavation depth, H_e (m)
Beneath the basement centre	68%	SW, DW (0.6, 0.96 and 1.5 m), RW	2	9
			3	15
At the side of the basement	69%	DW (0.96 m)	2	9
	70%	SW		

DW: diaphragm wall; SW: sheet pile wall; RW: rigid wall

Table 4. Summary of material parameters adopted for finite element analysis (Ng et al., 2013a; 2013b)

Angle of internal shearing resistance at critical state, φ'_c (°) [a]	30
Hardness of granulates, h_s (GPa) [a]	2.6
Exponent, n [a]	0.27
Minimum void ratio at zero pressure, e_{do} [a]	0.61
Critical void ratio at zero pressure, e_{co} [a]	0.98
Maximum void ratio at zero pressure, e_{io} [a]	1.10
Exponent, α [b]	0.14
Exponent, β [b]	3
Parameter controlling initial shear modulus upon 180° strain path reversal, m_R [b]	8
Parameter controlling initial shear modulus upon 90° strain path reversal, m_T [b]	4
Size of elastic range, R [b]	2×10^{-5}
Parameter controlling degradation rate of stiffness with strain, β_r [b]	0.1
Parameter controlling degradation rate of stiffness with strain, χ [b]	1.0
Coefficient of at-rest earth pressure, K_o	0.5

[a]: Obtained from Herle and Gudehus (1999)
[b]: Calibrated from triaxial test results for Toyoura sand (Maeda and Miura, 1999; Yamashita et al., 2000)
φ'_c: Determined from angle of repose test

Figures

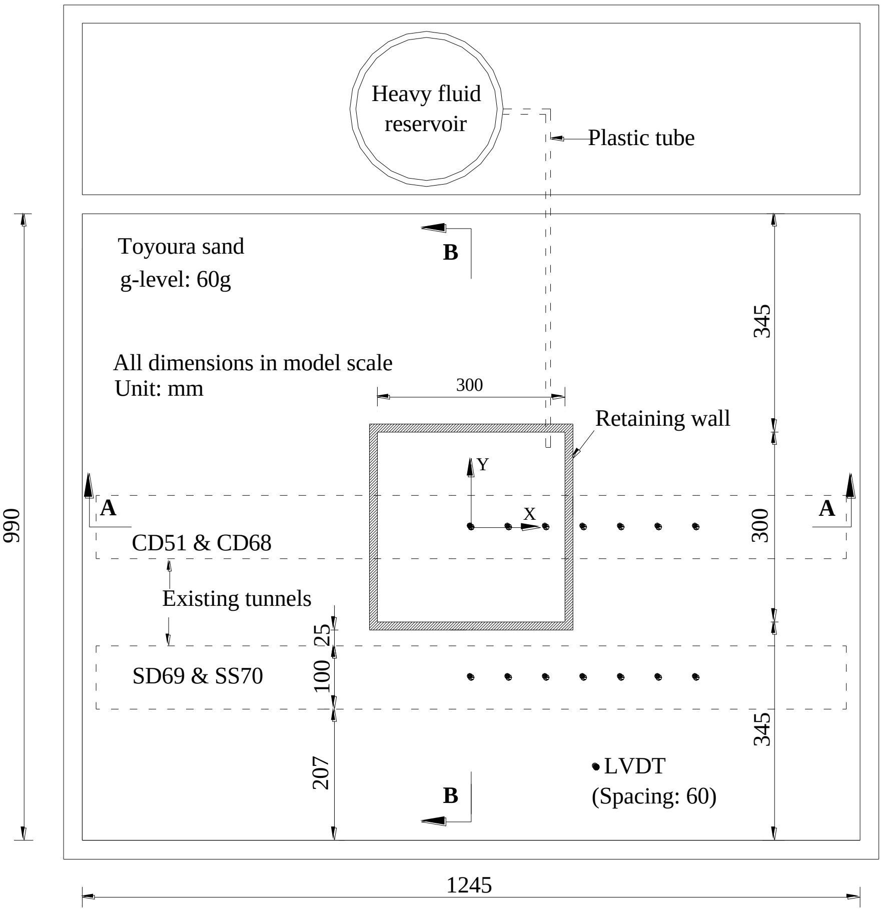

Fig. 1. Plan view of the centrifuge model

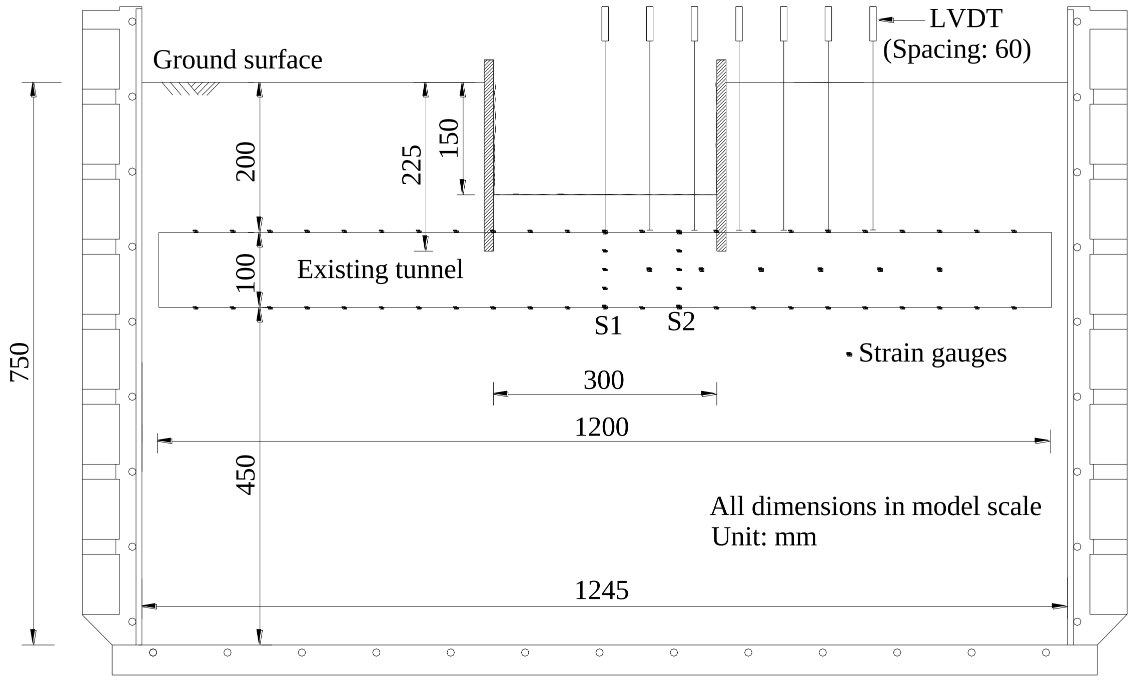

(a)

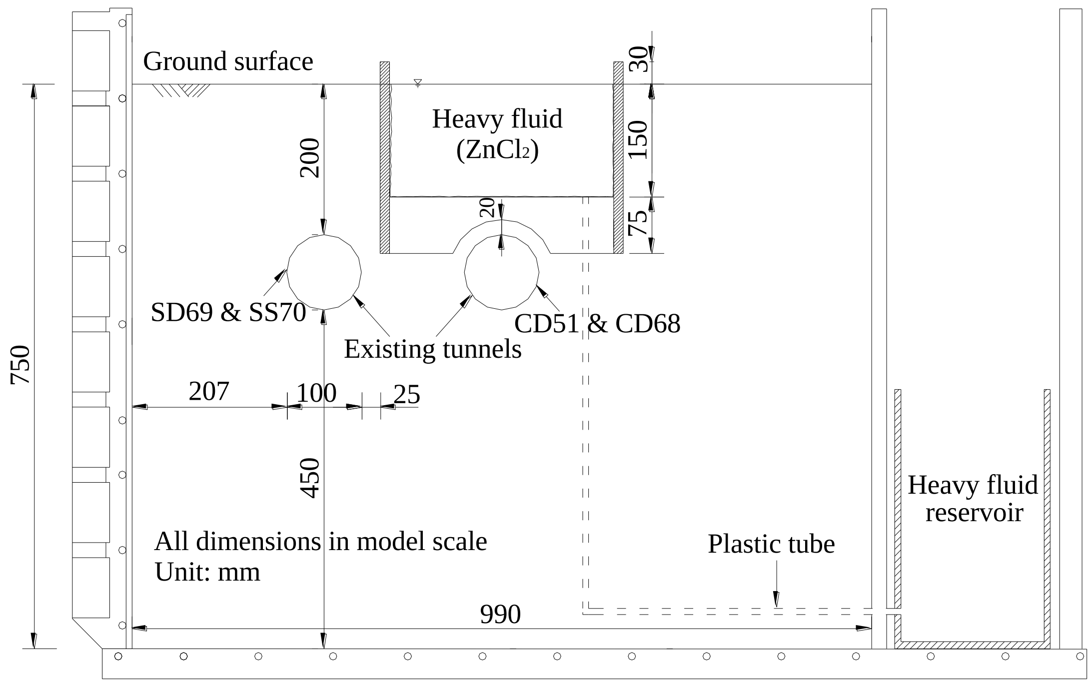

(b)

Fig. 2. Elevation views of the centrifuge model: (a) section A-A and (b) section B-B

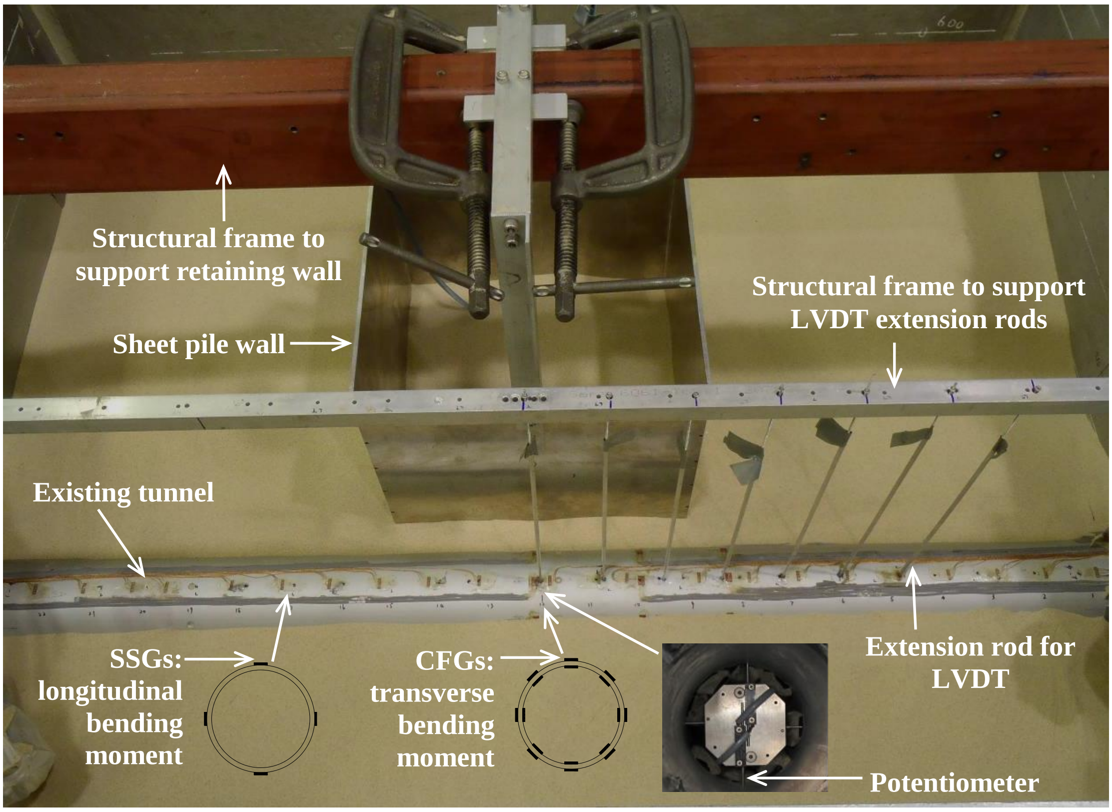

(a)

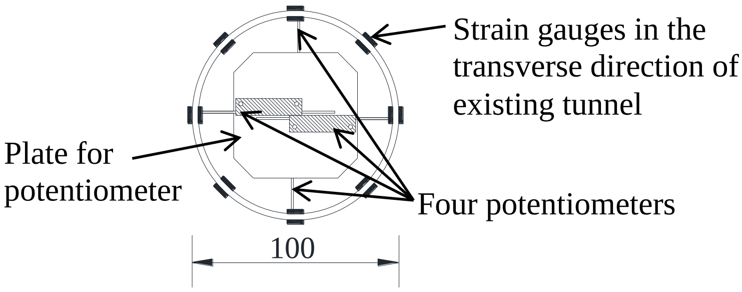

(b)

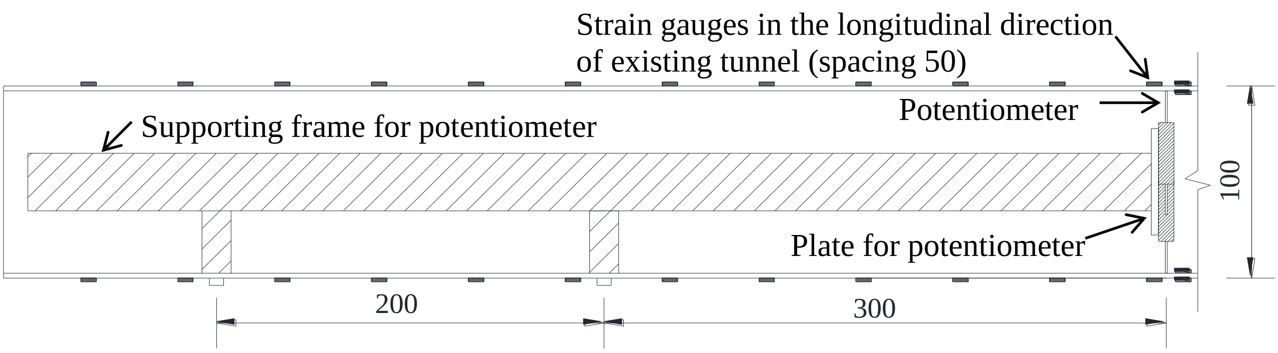

(c)

Fig. 3. (a) Types and locations of instruments installed on the existing tunnel; (b) Transverse section view; (c) Longitudinal section view (Unit: mm. All dimensions in model scale)

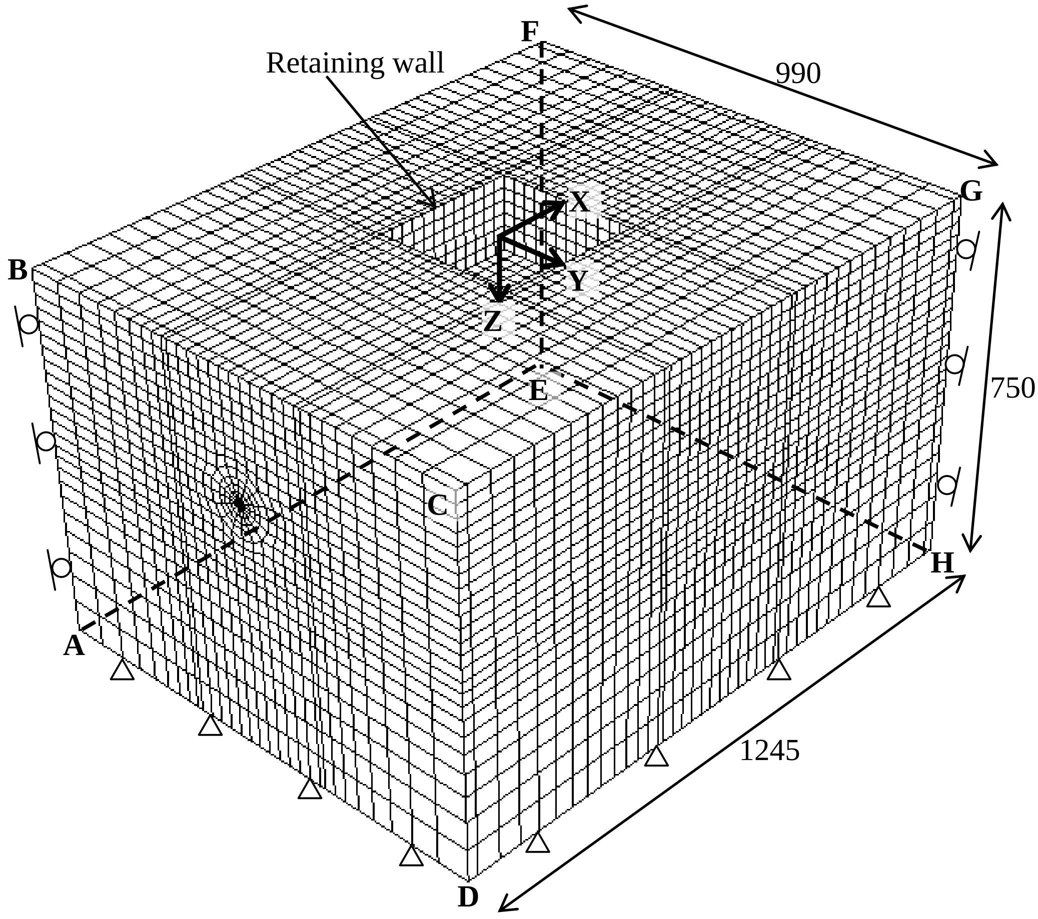

(a)

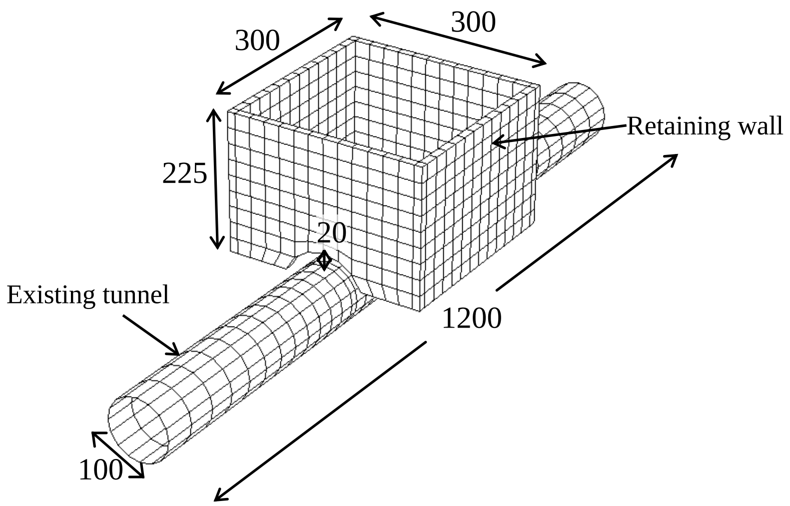

(b)

Fig. 4. (a) The three-dimensional finite element mesh adopted in this study; (b) Intersection of the tunnel and the retaining wall in detail (Unit: mm. All dimensions in model scale)

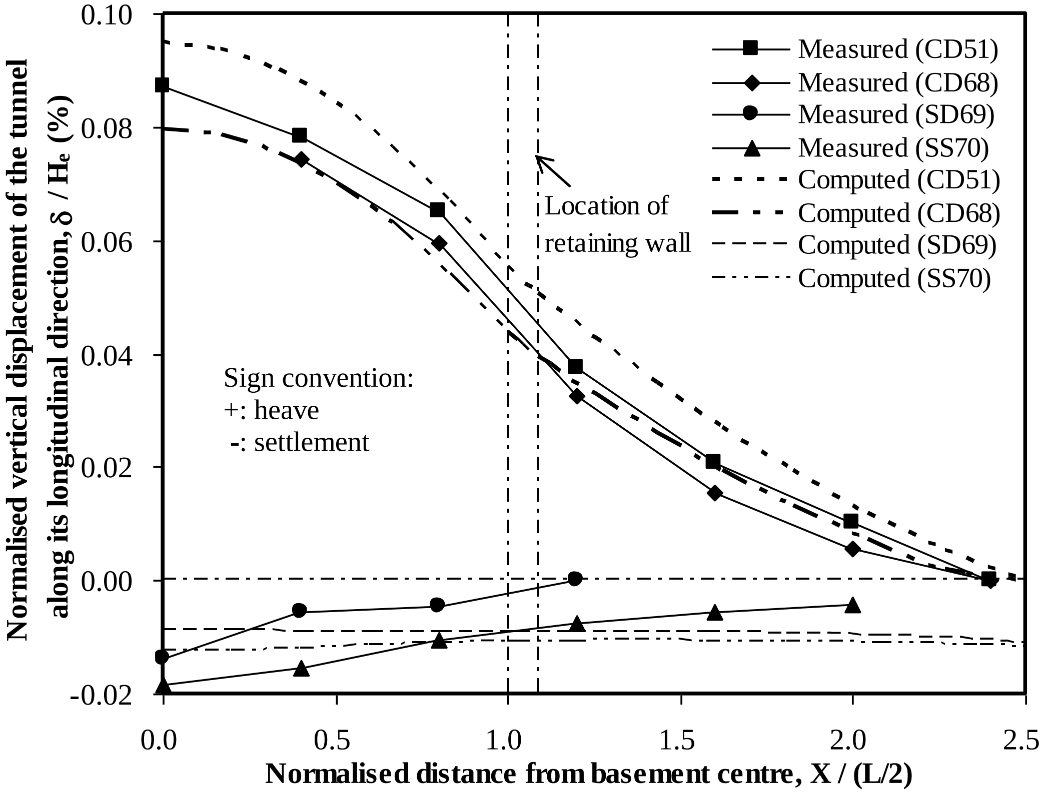

Fig. 5. Normalised vertical displacement of the tunnel along its longitudinal direction

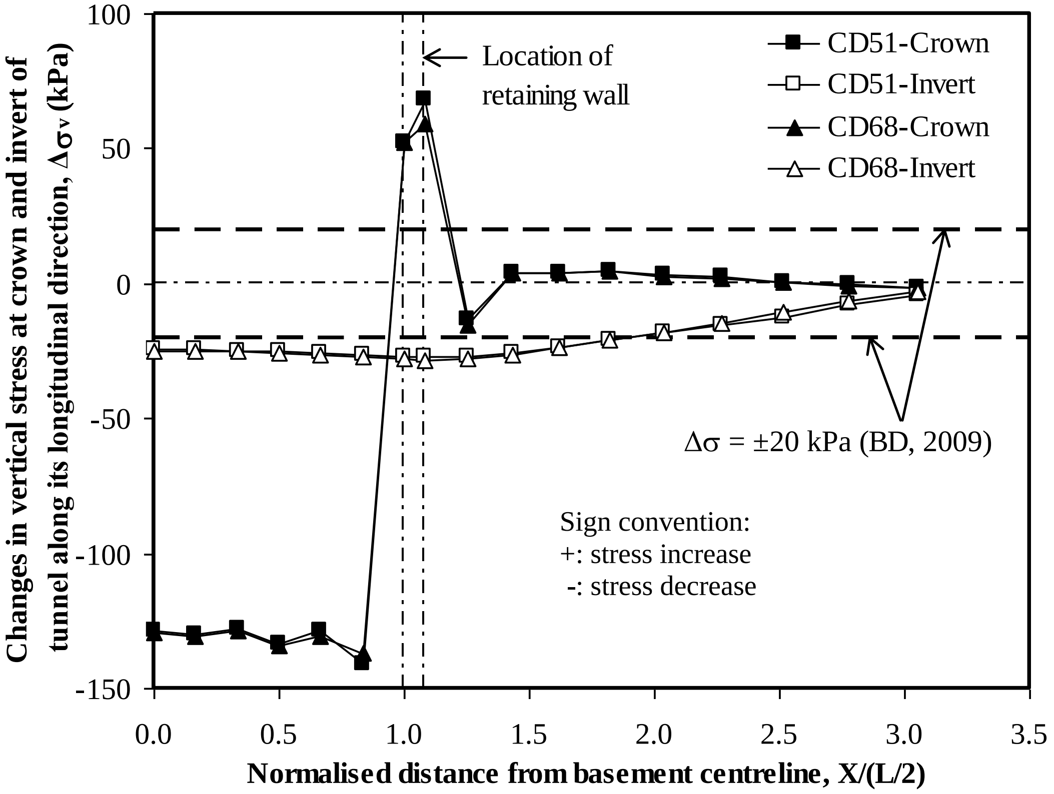

(a)

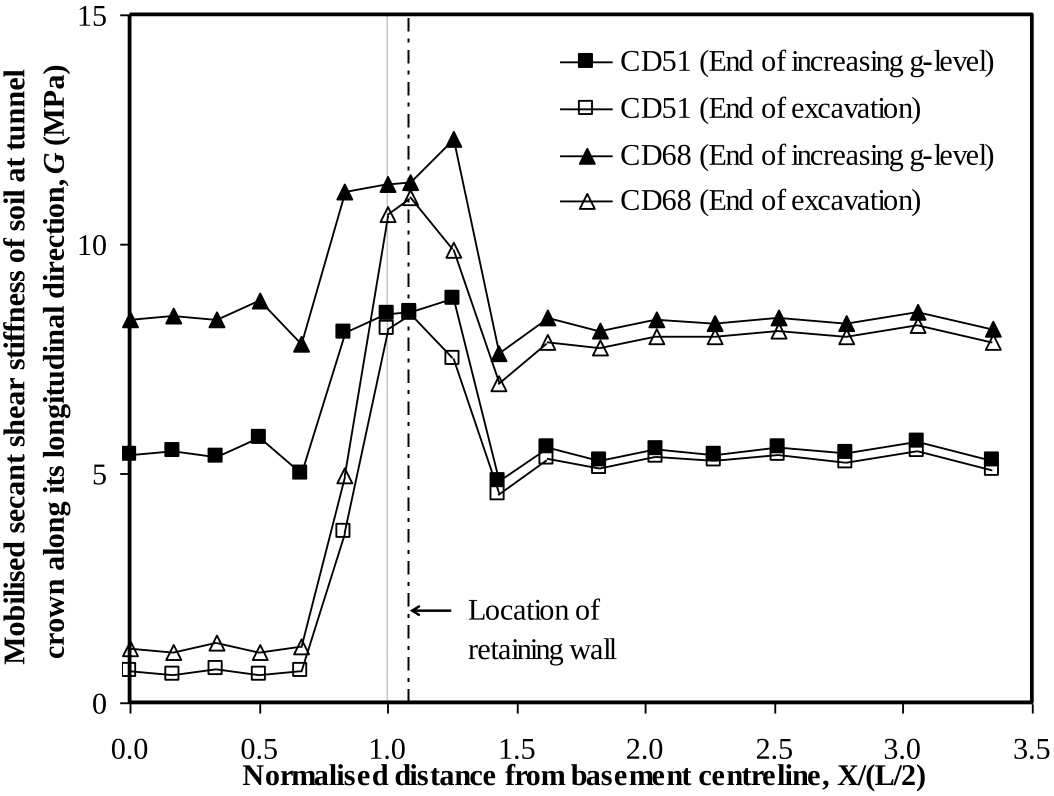

(b)

Fig. 6. Computed soil responses around the tunnel: (a) changes in vertical stress at the crown and invert; (b) mobilised secant shear stiffness of soil at the crown

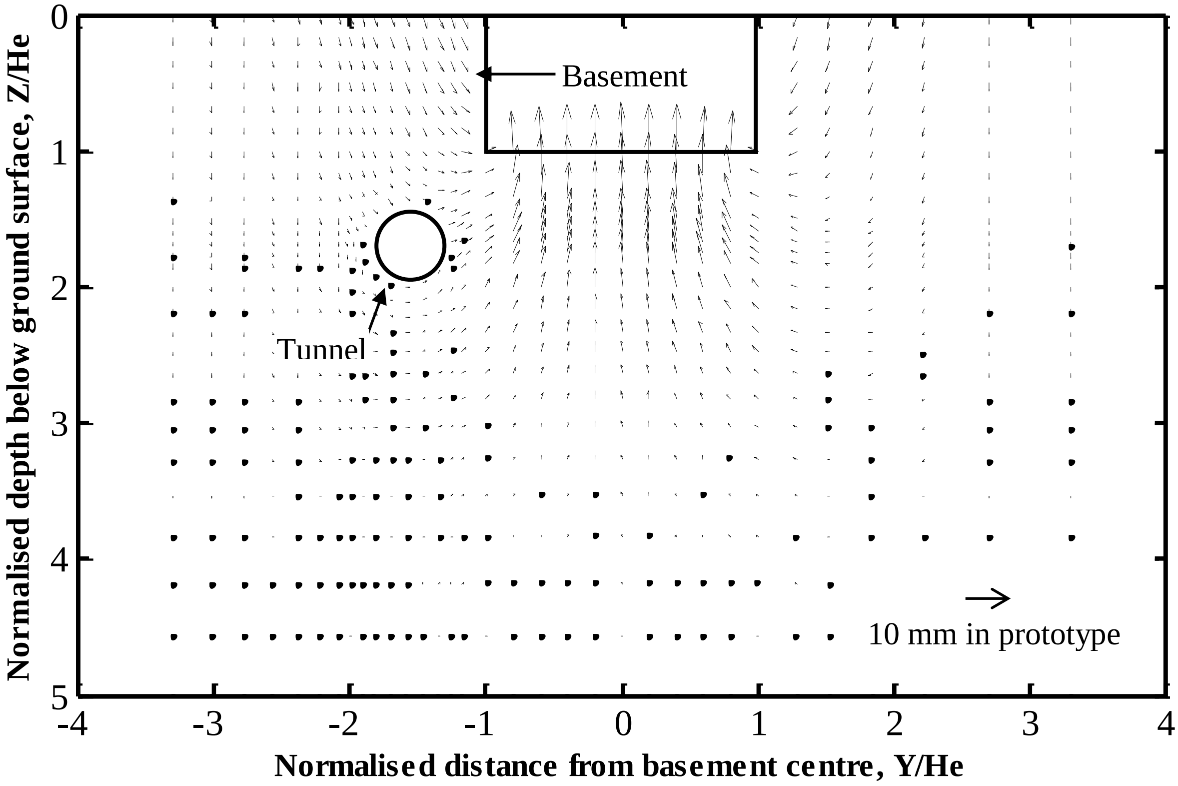

(a) Basement supported by a diaphragm wall

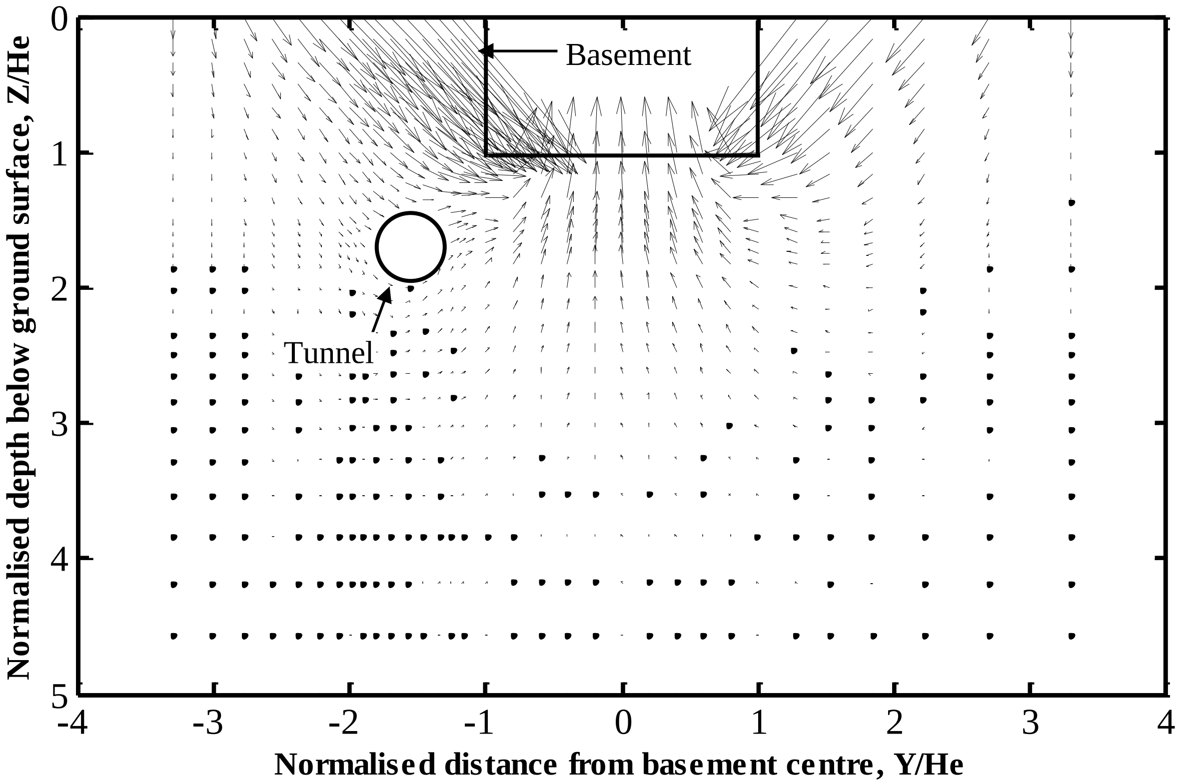

(b) Basement supported by a sheet pile wall

Fig. 7. Computed soil displacement vectors around the basement and the tunnel

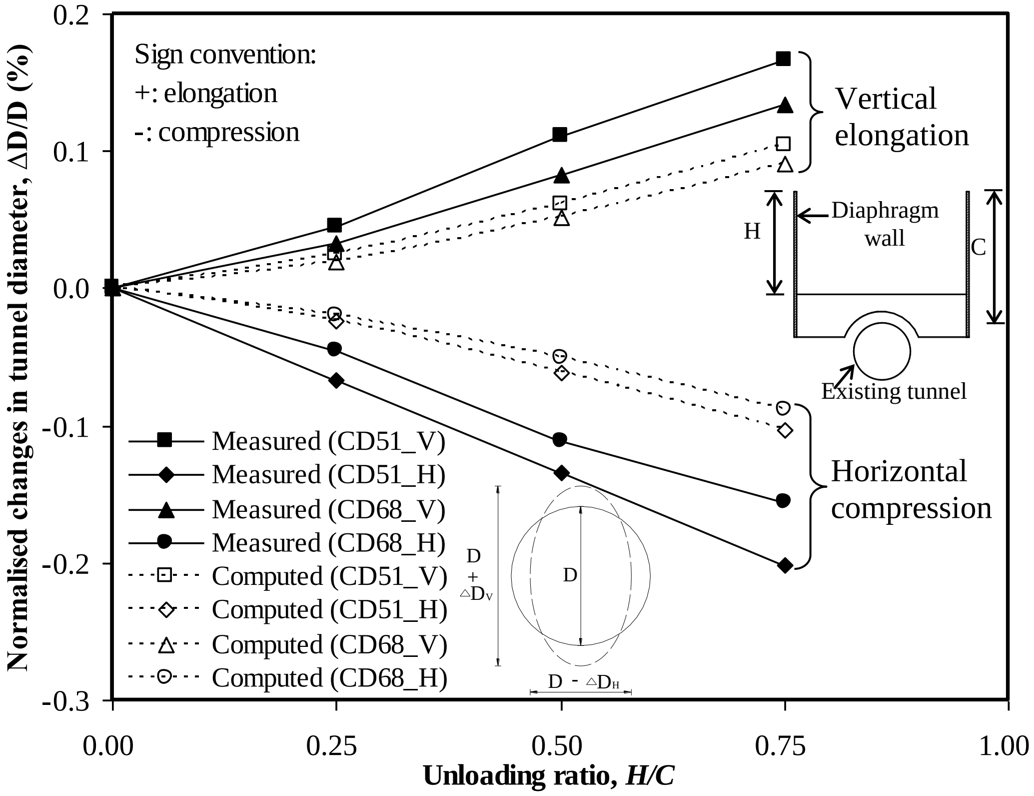

Fig. 8. Elongation and compression of the tunnel located beneath the basement centre

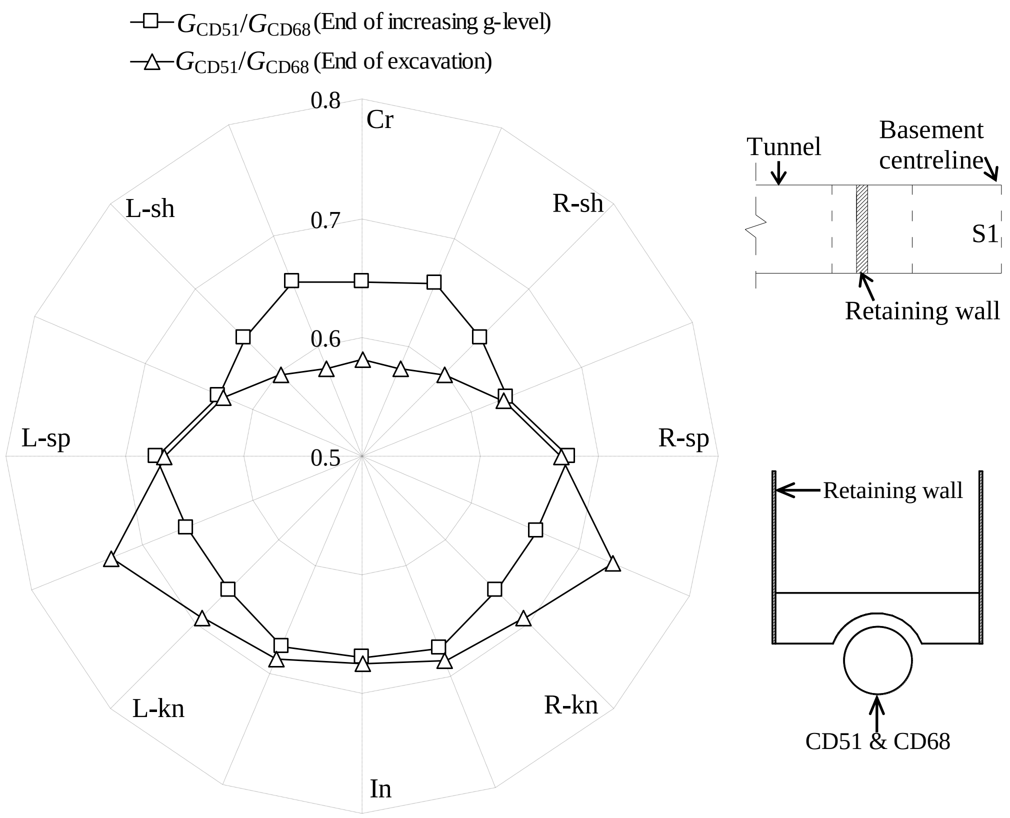

Fig. 9. Mobilised secant shear stiffness of soil along the transverse direction of the tunnel in section S1

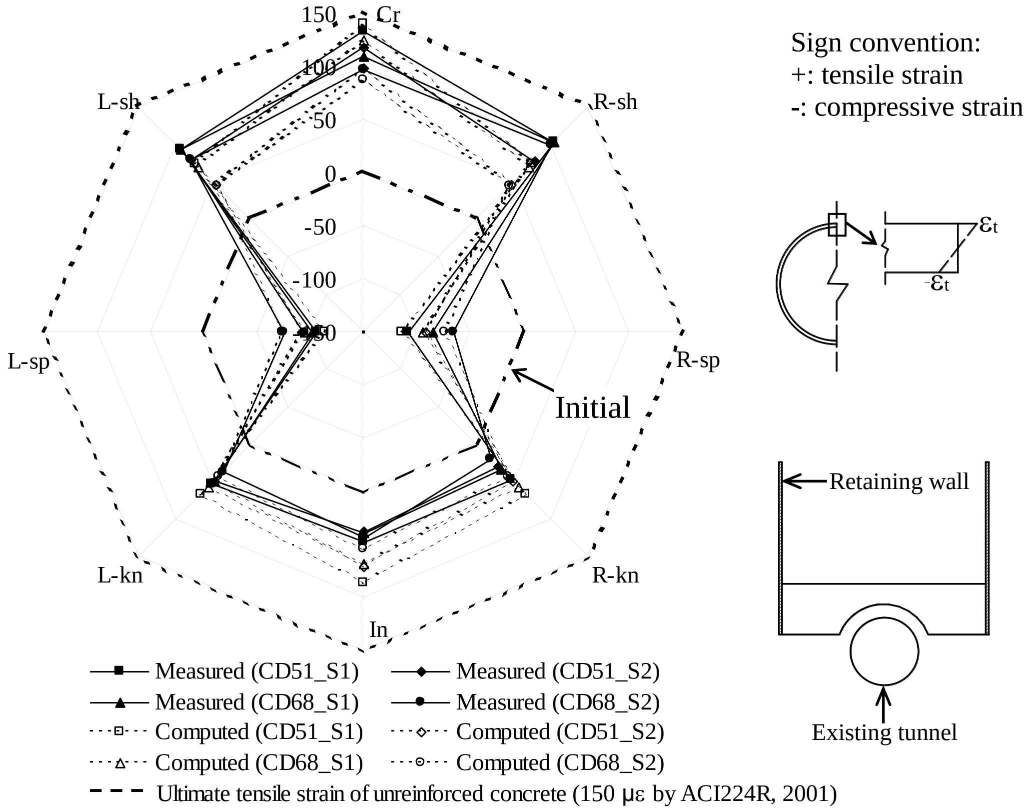

(a) Influence of sand density

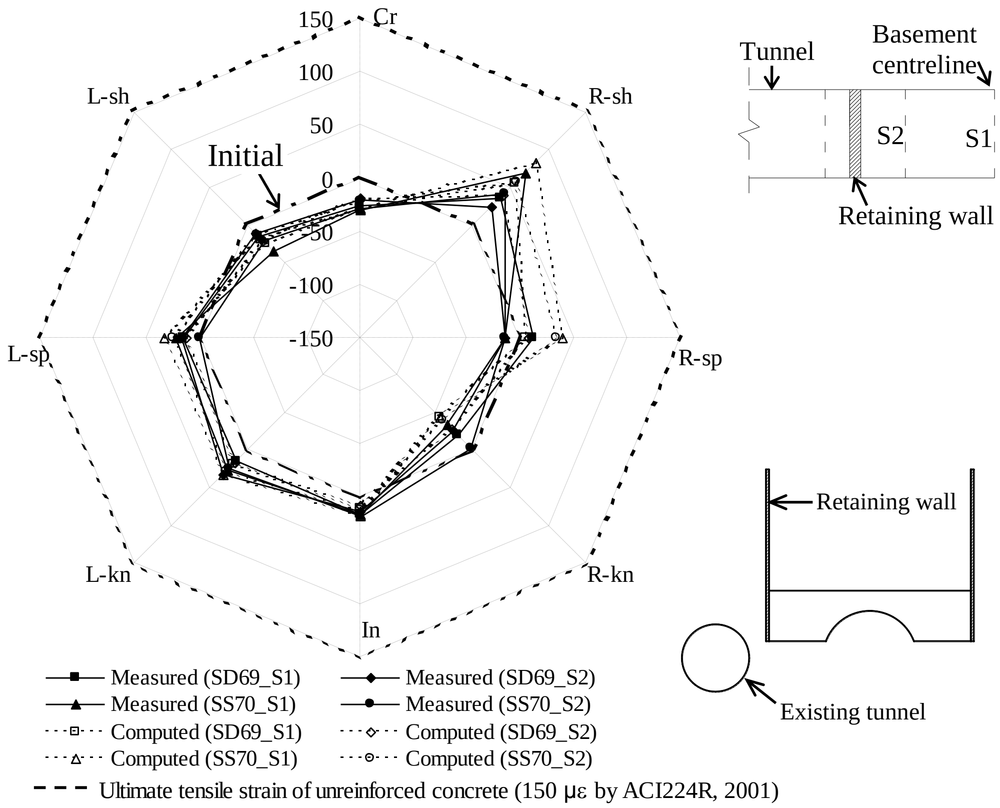

(b) Influence of flexural stiffness of retaining wall

Fig. 10. Induced strain at the outer surface of the tunnel along its transverse direction

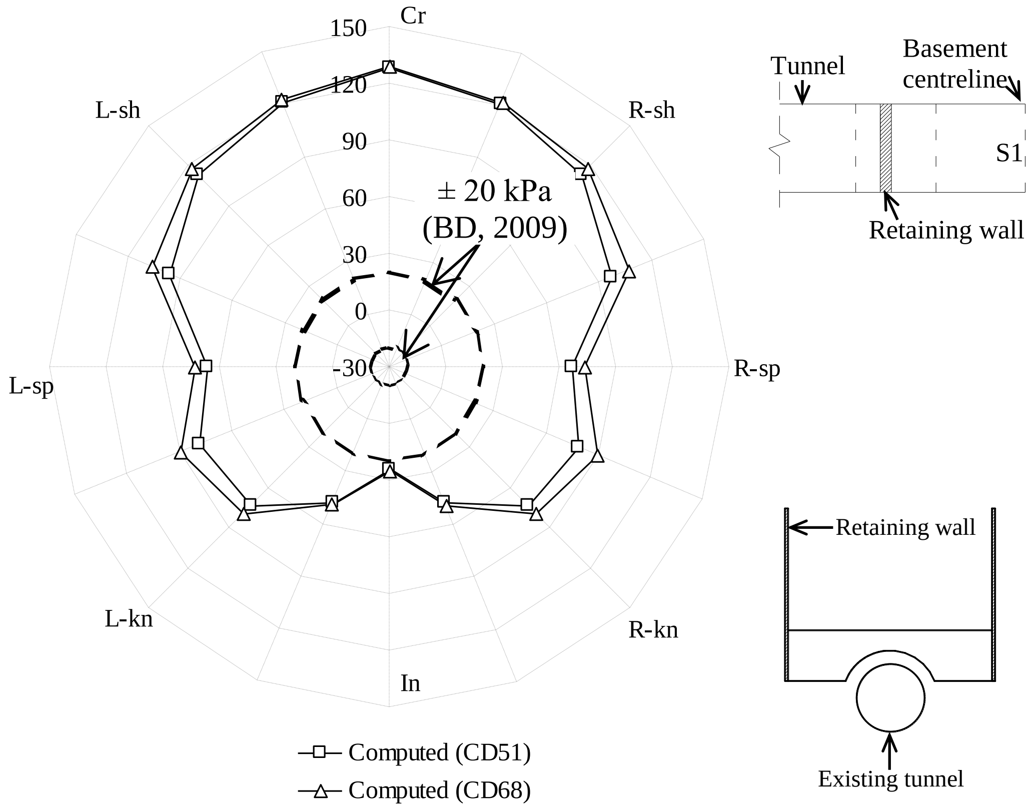

(a) Influence of sand density

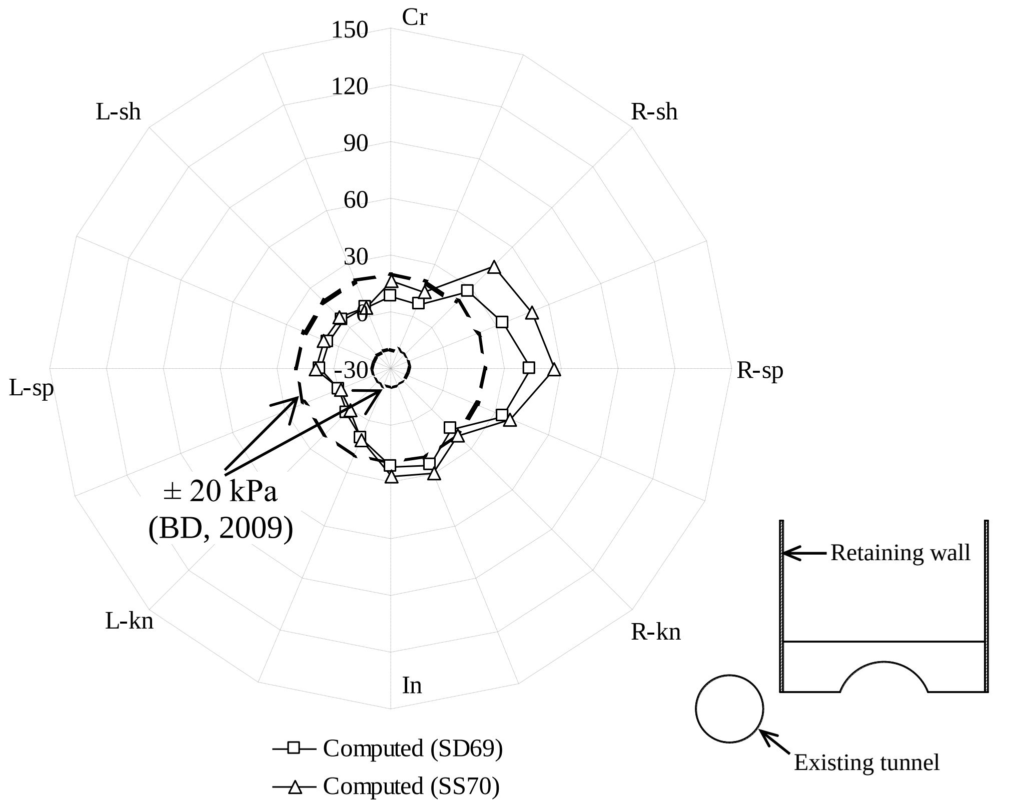

(b) Influence of flexural stiffness of retaining wall

Fig. 11. Reduced normal stress acting on the tunnel lining in section S1 (Unit: kPa)

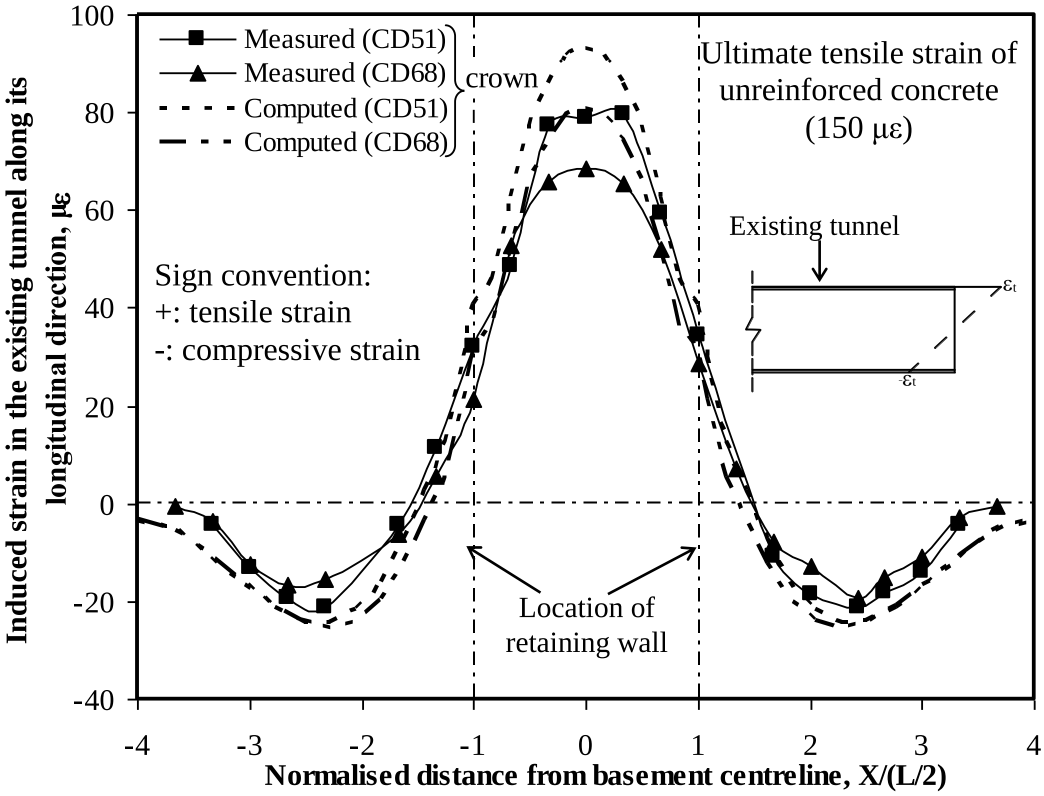

Fig. 12. Effects of sand density on induced strain in the tunnel along its longitudinal direction

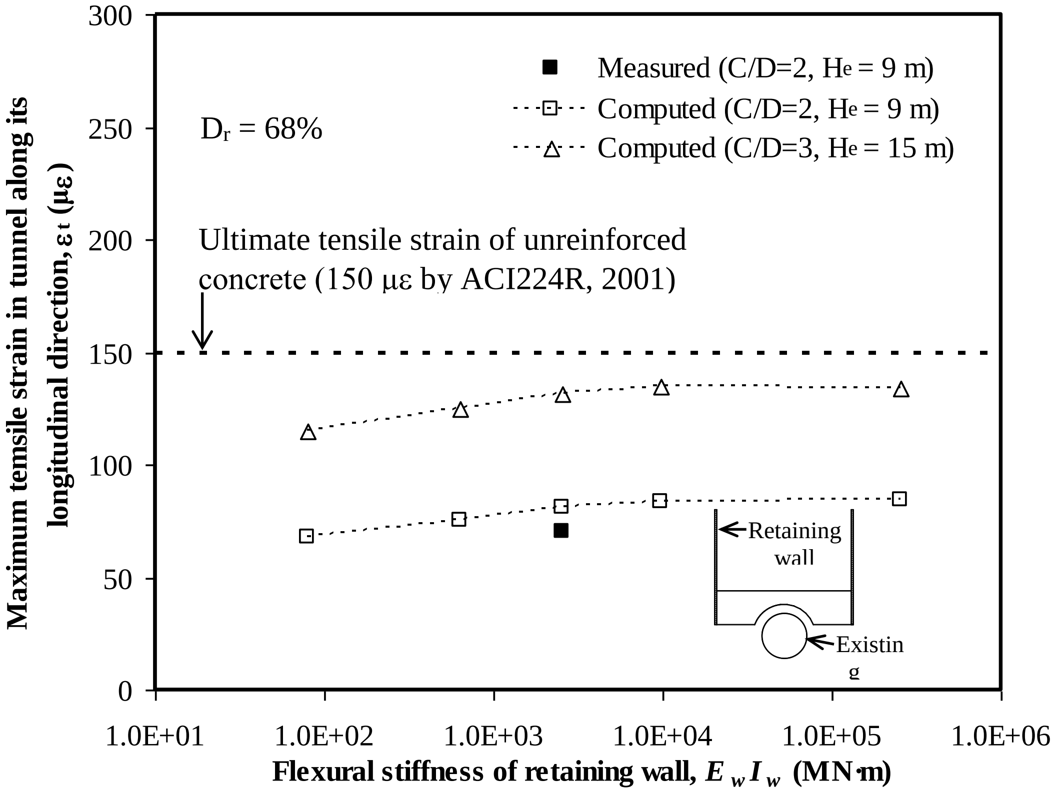

(a) Maximum tensile strain in tunnel along its longitudinal direction

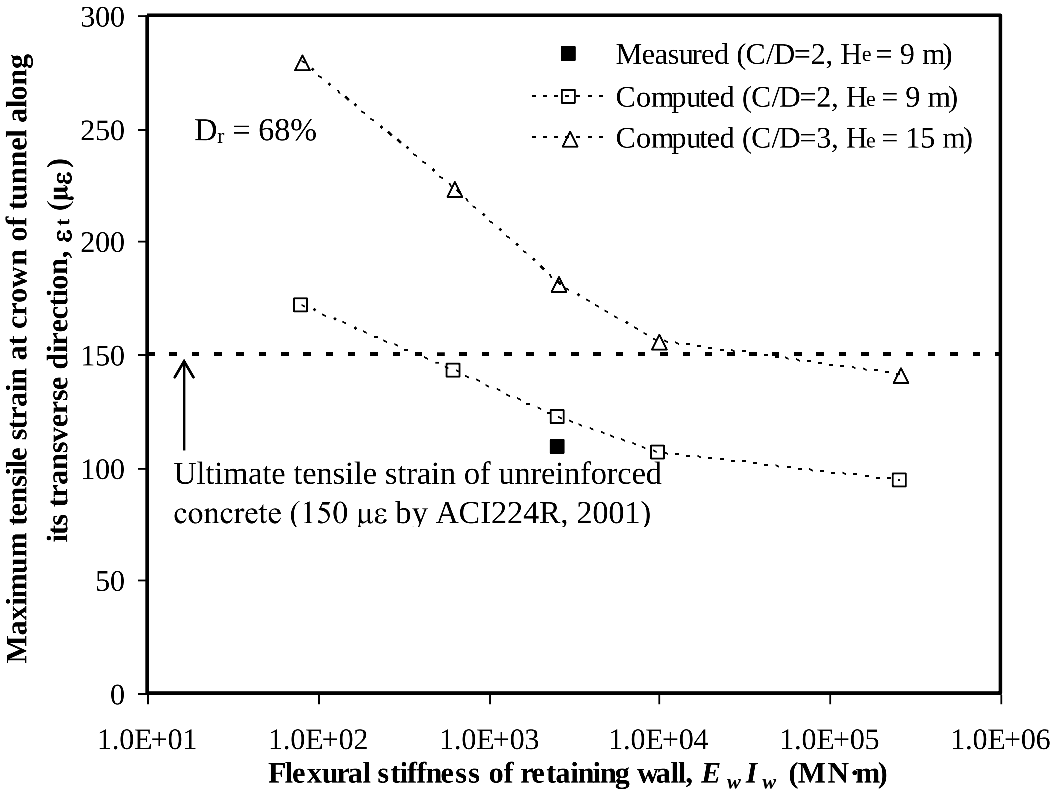

(b) Maximum tensile strain at crown of tunnel along its transverse direction

Fig. 13. Effects of wall stiffness on three-dimensional tensile strains induced in the tunnel by basement excavation